Stony Brook University

Transverse Momentum Distribution for Drell Yan Process

A Thesis presented

by

Yikun Wang

to

The Graduate School

in Partial Fulfillment of the

Requirements

for the Degree of

Master of Arts

in

Physics

Stony Brook University

August 2014

Stony Brook University

The Graduate School

Yikun Wang

We, the thesis committe for the above candidate for the

Master of Arts degree, hereby recommend

acceptance of this thesis

Patrick Meade
Assistant Professor, the Department of Physics and Astronomy

George Sterman
Professor, the Department of Physics and Astronomy

John Hobbs
Professor, the Department of Physics and Astronomy

This thesis is accepted by the Graduate School

Charles Taber
Dean of the Graduate School

Abstract of the Thesis

Transverse Momentum Distribution for Drell Yan Process

by

Yikun Wang

Master of Arts

in

Physics

Stony Brook University

2015

The Drell-Yan process is the production of massive lepton pairs in hadronic collisions. In this thesis, we investigate the transverse momentum distribution of the intermediate vector bosons for the Drell-Yan process. This distribution can be predicted by perturbative QCD. However, one difficulty of the calculation is large logarithms that occur in the calculation of the differential cross section which come from the soft and collinear structure of the phase space. The large logarithmic terms in the differential cross section spoil the validity of perturbative expansion in the region of small transverse momentum. Transverse momentum resummation can give convergent results and reliable perturbative predictions by summing over the logarithmic contributions. In this thesis we review and calculate the resummed transverse momentum distribution for the Drell-Yan process up to leading and next leading logarithmic level. Another approach to predicting the transverse momentum distribution is the parton shower algorithm in Monte Carlo event generators. Parton shower algorithms can simulate the soft and collinear emissions from incoming and outgoing partons of the process. The logarithmic accuracy of the parton shower algorithm is analyzed in this thesis. The numerical comparison between the parton shower prediction and the resummation logarithmic accuracy is made accordingly.

Table of Contents

1 Introduction **1**
- 1.1 QCD Symmetries and Lagrangian . . . 1
- 1.2 Asymptotic Freedom . . . 3
- 1.3 Perturbative QCD . . . 4

2 Drell Yan Process **7**
- 2.1 Drell Yan Mechanism . . . 8
- 2.2 Factorization of Drell Yan Process . . . 9
- 2.3 Transverse Momentum Distribution . . . 10

3 Transverse Momentum Resummation **17**
- 3.1 DDT Formula . . . 17
- 3.2 Resummation from Back-to-back Jets . . . 19
- 3.3 A formalism with Universal Form Factor . . . 22

4 Parton Shower Algorithms **26**
- 4.1 Final State Radiation . . . 26
- 4.2 Initial State Evolution . . . 28
- 4.3 Large Quark Mass Effects . . . 28

5 Logarithmic Accuracy of Parton Shower Algorithms **30**
- 5.1 Higher Accuracy Logarithmic Resummation Approaches of Parton Shower . . . 30
  - 5.1.1 Soft Emissions and Coherence Effects . . . 30
  - 5.1.2 Color Information and Dipole Approach . . . 31
  - 5.1.3 Matching with ME and NLO . . . 31
- 5.2 Transverse Momentum Distribution of Z Boson for Drell Yan Process: Resummation . . . 33
- 5.3 Logarithmic Resummed Accuracy of Pythia8 Prediction for Transverse Momentum Distribution . . . 37

6 Conclusion **40**

List of Figures

1 Running couplings of the Standard Model: α_s is the coupling of QCD, α is the coupling of electromagnetic interaction, α_w is the coupling of weak interaction. 5
2 Drell Yan process in the parton model. The hard process in this figure is at leading order (LO) with γ being the intermediate state. 8
3 Leading order and next leading order diagrams for Drell Yan process [23]. 10
4 NLO corrections to $q\bar{q} \to Z$: real emission of gluons 11
5 NLO q_T distribution of $q\bar{q} \to Z$ at 14TeV 14
6 NLO corrections to $q\bar{q} \to Z$: virtual gluons 14
7 Ladder structure of the soft and collinear emissions for Drell Yan Process 18
8 Rules of the color flow construction in parton shower 31
9 Logarithmic resummation accuracy of parton shower with ME/NLO corrections. (a) parton shower with ME matching. The blob is half-filled because that only real emission corrections are included; (b) parton shower with NLO matching (c) parton shower with multi-jets merging, where the half-filled blobs is due to that only real emissions above the merging scale are included. 32
10 Resummation of Z boson transverse momentum distribution for Drell Yan process at NLL accuracy with different factorization scales at $E_{CM} = 14$TeV. 38
11 Comparison with the ResBos NLL resummation of the Z boson transverse momentum distribution for Drell Yan process: $E_{CM} = 14$TeV, $\mu_F = m_Z$ 38
12 Numerical comparison between the Pythia8 prediction and the resummation predictions at LL and NLL accuracy with $E_{CM} =$ 14TeV. 39

Chapter 1 Introduction

The Standard Model is the theory of elementary particles and their interactions. There are two building blocks in the Standard Model, the electroweak theory with spontaneous broken $SU(2) \times U(1)$ gauge group, and the non-Abelian theory of quantum chromodynamics, or QCD, with unbroken $SU(3)$ gauge group. QCD describes the strong interactions between quarks and gluons. It has been confirmed by various experimental tests ever since 1960's. One big success of QCD is the prediction of physics at colliders, which involve various processes with strong interactions.

This chapter firstly gives a general description of the theory of QCD in the Standard Model, including the QCD Lagrangian and one of its key features, asymptotic freedom. The second part is an introduction to the perturbative method of QCD, which is valid and responsible for the first principle calculation of QCD at short distances.

1.1 QCD Symmetries and Lagrangian

The symmetry group of QCD is the non-Abelian SU(3) gauge group. The group has eight generators, which correspond to the eight gauge bosons, called gluons, of QCD. The gluon fields are octets under the SU(3) gauge group.

QCD has an additional colour degree of freedom [1, 2], whose index is denoted by i and carried by each of the six quarks. The quark fields with colour indices are in fundamental representation of the local SU(3) group, which is symmetry group of the colour degree of freedom. There are accordingly three colors, say red, green, blue for $i = 1, 2, 3$. Quark fields are then 3-vectors under the local SU(3) group.

Another symmetry of QCD is the approximate symmetry of flavors, which is however not exact. There are six flavors of quarks found till now, which are called up (u), down (d), charm (c), strange (s), top (t) and bottom (b). They are divided into three generations similar as the case of leptons. The local symmetry of flavors is chiral and varies at different energy scales. It is related to the number of massless flavors N_f at a certain scale.

The classical Lagrangian of QCD is

$$\mathcal{L}_{\text{classical}} = \bar{\psi}^i_{\text{q}} i \not{D}_{ij} \psi^j_{\text{q}} - m_{\text{q}} \bar{\psi}^i_{\text{q}} \psi_{\text{q},i} - \frac{1}{4} F^a_{\mu\nu} F^{a,\mu\nu}, \tag{1}$$

where $\psi_{\rm q}^i$ is the quark field with colour index i, $F_{\mu\nu}^a$ is the gluon field strength tensor with adjoint index $a = 1, ..., 8$ (the summation over a is understood), and $\not{D}_{ij} = \gamma_\mu D_{ij}^\mu$. The QCD covariant derivative D^μ is

$$D_\mu = \partial_\mu - ig_{\rm s} t^a A_\mu^a, \tag{2}$$

where $g_{\rm s}$ is the strong coupling, A_μ^a is the gluon field, and the generators $t^a = \frac{1}{2}\lambda^a$ with λ^a being the three-dimensional hermitian and traceless Gell-Mann matrices of SU(3) (the summation over a is understood).

C_F and C_A are two important parameters in QCD originating from the group structure. They are defined as

$$\begin{aligned} \sum_a t_{ij}^a t_{jk}^a &= C_F \delta_{ik},\ C_F = \frac{N_c^2 - 1}{2N_c} \\ \sum_{ab} f^{abc} f^{abd} &= C_A \delta^{cd},\ C_A = N_c. \end{aligned} \tag{3}$$

where f^{abc} is the structure constant of the adjoint representation of SU(3) and N_c is the number of quark generations. They always show up as factors in the colour summed matrix elements.

Since the gauge fields have an unphysical degree of freedom, to define propagators of the gauge fields, one needs to add a gauge fixing term in the QCD Lagrangian to eliminate the extra degree of freedom. The gauge fixing term is of the general form

$$\mathcal{L}_{\text{gauge fixing}} = -\frac{1}{2\xi}(\partial^\mu A_\mu^a)^2, \tag{4}$$

where ξ is the gauge parameter. Physics is invariant under different choices of ξ, even though the calculation can be quite different. The case of $\xi = 1$ is known as Feynman gauge and the case of $\xi = 0$ is known as Laudau gauge.

Although physics is independent of ξ, this does not manifest itself in a non-Abelian theory like QCD at the quantum level. To guarantee the invariance, an additional so called ghost field and a corresponding ghost term in the Lagrangian are introduced to the theory. The ghost term in the QCD Lagrangian is

$$\mathcal{L}_{\text{ghost}} = \bar{c}^a(-\partial^2 \delta^{ac} - g_{\rm s}\partial^\mu f^{abc} A_\mu^b) c^c, \tag{5}$$

where c^a is the ghost field and f^{abc} is structure constant of the SU(3) adjoint representation.

Finally, the QCD Lagrangian is totally

$$\mathcal{L}_{\rm QCD} = \mathcal{L}_{\rm classical} + \mathcal{L}_{\rm gauge\ fixing} + \mathcal{L}_{\rm ghost}. \tag{6}$$

Having included all necessary ingredients, now the theory can be quantized as usual and the Feynman rules are defined accordingly.

1.2 Asymptotic Freedom

Asymptotic freedom [3, 4] is one of the most important features of QCD. It guarantees that QCD can be calculated perturbatively at high energy scales, or equivalently short distances. This is because the energy scale dependent running coupling of QCD is smaller and smaller when the energy scale goes higher and higher, while the smallness of coupling "constants" is the foundation of perturbation theory.

To avoid ultraviolet divergences, QCD is renormalized according to the renormalization theory. The renormalization group equations (RGE) are given based on the variation of renormalization scales. They show explicitly how physics changes with respect to the running of the energy scale. More specifically, the differential equations of RGE are obtained by keeping the bare couplings, i.e. couplings in the bare Lagrangian, or physical quantities measured at the energy scale Q invariant under the arbitrarily chosen of renormalization scale. The RGE of a physical quantity R is

$$\big[\mu^2\frac{\partial}{\partial\mu^2} + \beta(\alpha_{\rm s})\frac{\partial}{\partial\alpha_{\rm s}} - \gamma_m(\alpha_{\rm s})m\frac{\partial}{\partial m}\big]R(\frac{Q^2}{\mu^2}, \alpha_{\rm s}, \frac{m}{Q}) = 0, \tag{7}$$

where Q is the physical scale, μ is the renormalization scale, $\alpha_{\rm s} \equiv g_{\rm s}^2/4\pi$, $\gamma_m(\alpha_{\rm s})$ is the anomalous dimension, and $\beta(\alpha_{\rm s})$ is the beta function defined as

$$\beta(\alpha_{\rm s}) = \frac{\partial\alpha_{\rm s}}{\partial{\rm ln}\mu^2}. \tag{8}$$

The β function illustrates how the coupling $\alpha_{\rm s}$ is dependent on the energy scale μ. This is called the running behavior of $\alpha_{\rm s}$. The beta function can be expanded perturbatively

$$\beta(\alpha_{\rm s}) = -\alpha_{\rm s}\sum_{n=0}^{\infty}\beta_n\big(\frac{\alpha_{\rm s}}{4\pi}\big)^{n+1}, \tag{9}$$

where β_n's are computed order by order according to Feynman diagrams. The first two terms of β_n are

$$\begin{aligned}\beta_0 &= \frac{1}{3}(11C_A - 2N_f),\\ \beta_1 &= \frac{2}{3}(17C_A^2 - 5C_A N_f - 3C_F N_f),\end{aligned} \tag{10}$$

which correspond to one-loop and two-loop diagrams respectively. N_f, C_A and C_F in Eqs. (10) have been defined above as important coefficients of QCD.

The minus sign in Eq. (8) is crucial. It gives the behavior of the coupling decreasing as μ increasing. For example, the solution of Eq. (8) with only the first order term β_0 included is

$$\begin{aligned}\alpha_{\rm s}(\mu^2) &= \frac{\alpha_{\rm s}(\mu_0^2)}{1 + (\beta_0/4\pi)\alpha_{\rm s}(\mu_0^2)\ln(\mu^2/\mu_0^2)}\\ &= \frac{4\pi}{\beta_0 \ln(\mu^2/\Lambda_{\rm QCD}^2)},\end{aligned} \tag{11}$$

where $\Lambda_{\rm QCD} \equiv \mu_0 e^{-2\pi/(\beta_0 \alpha_{\rm s}(\mu_0^2))}$ is the characteristic scale of QCD, at which the coupling constant $g_{\rm s}$ is of order one, say $g_{\rm s} \sim \mathcal{O}(1)$. One can see clearly the asymptotic free behavior of $\alpha_{\rm s}$ from this expression. Accordingly, the non-perturbative region of QCD is $Q \lesssim \Lambda_{\rm QCD}$ and the perturbative QCD valid region is $Q \gg \Lambda_{\rm QCD}$.

Asymptotic freedom is unique for the non-Abelian theory. As an Abelian gauge theory, for example, the coupling of QED is not asymptotic free. Fig. 1.2 shows running behaviors of interactions in the Standard Model.

1.3 Perturbative QCD

Although QCD is asymptotically free at high energy scales, its coupling is stronger and stronger at low energy scales, which will invalidate the perturbative argument. Due to the strong coupling strength at such scales, new quarks and gluons will be easily created and all together form physically observable particles, like hadrons. This phenomenon is called confinement, which is another important feature of QCD.

Although confinement prevents us from calculating QCD processes using solely the perturbative approach, the parton model [5, 6] can describe confinement of partons using parton distribution functions (PDF). Partons are

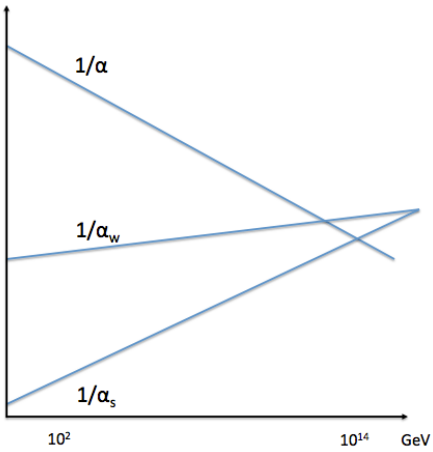

Figure 1: Running couplings of the Standard Model: $\alpha_{\rm s}$ is the coupling of QCD, α is the coupling of electromagnetic interaction, $\alpha_{\rm w}$ is the coupling of weak interaction.

point-like particles in the parton model and are now interpreted as quarks and gluons in the Standard Model. The PDF's only depend on Bjorken scaling variable [7, 8, 9], which is defined as

$$x \equiv \frac{-q^2}{2p \cdot q}, \tag{12}$$

where p is the momentum of hadrons and q is the transferred momentum between hadrons and testing particles (for example lepton in deep inelastic scattering (DIS)).

For hadron-hadron collisions, the total cross section of a process F can be written in terms of the PDF's and the so-called partonic or hard cross section

$$\sigma^{\rm F}_{h_1,h_2} = \Sigma_{a,b} \int_0^1 dx_1 dx_2 f_{a/h_1}(x_1) f_{b/h_2}(x_2) \sigma^{\rm F}_{a,b}, \tag{13}$$

where h_1 and h_2 are incoming hadrons, a and b denote parton flavors, x_1, x_2 are Bjorken scaling variables, and $\sigma^{\rm F}_{a,b}$ is the partonic cross section for the hard process F in ab channel. The parton distribution functions $f_{a/h}(x)$ are universal for different processes. PDF's can not be predicted perturbatively. They are even difficult to be calculated using non-perturbative approaches

like lattice QCD. Thus the PDF's are usually obtained directly from experimental data.

Another difficulty of perturbative QCD is its infrared divergence. Most of the QCD processes are IR divergent due to the zero mass of gluons. IR divergences are not well defined even within the renormalized theory. However, certain methods of perturbative QCD can identify and regularize IR safe quantities. For example, the theory of factorization [10] can systematically factorize short distance and long distance behaviors into different parts. Then the IR safe quantities, which are independent of long distance behaviors, can be fully analyzed and calculated using perturbative approaches. The factorization theory will be described in more detail for Drell Yan process in the next chapter.

Chapter 2 Drell Yan Process

Drell Yan process is the production of massive lepton pairs via the production of electroweak vector bosons at hadronic colliders [11]. As the intermediate vector bosons are timelike, they can also be produced as physical particles. The process is important for the study of PDF and perturbative QCD. The agreement between the experimental Drell Yan cross section and its parton model prediction confirms the validity of parton model. The Drell Yan process has large production rates and clear signatures at hadronic colliders. Thus it can provide good experimental information on the PDF's.

According to the parton model, the produced lepton pairs of Drell Yan process are given by the annihilation of quark antiquark pairs coming from hadrons at the collider. Fig. 2 shows the structure of such an interpretation. The total cross section can be then written regarding the PDF

$$\sigma^{\mathrm{V}}_{\mathrm{h_1 h_2}} = \Sigma_{ab} \int_0^1 dx_1 \int_0^1 dx_2 f_{\mathrm{a/h_1}}(x_1) f_{b/h_2}(x_2) \hat{\sigma}^{\mathrm{V}}_{ab}, \tag{14}$$

where the superscript 'V' denotes the vector boson production of Drell Yan process, $\hat{\sigma}^{\mathrm{V}}_{ab}$ is partonic or hard process cross section, $f_{a/h_1}(x)$ and $f_{b/h_2}(x)$ are the universal PDF's, which can be extracted from the data of deep inelastic scattering (DIS). The hard process of Drell Yan can be calculated using perturbative QCD, although certain non-perturbative effects need to be taken into consideration. The factorization theorem guarantees that the inclusive partonic cross section is infrared safe.

The Born level cross section is purely electroweak, however, important QCD corrections arise from higher order diagrams of the hard process. Up to now, the QCD corrections have been calculated up to the next-to-next-to-leading order (NNLO) accuracy [12, 13].

The transverse momentum differential cross section of the produced vector bosons for Drell Yan process is an important distribution. It reveals collinear and soft structure of the semi-inclusive cross section.

This chapter firstly introduces the mechanism of Drell Yan process and its kinematic structure. The second section is a description of the factorization theorem for Drell Yan process. Then finally, we compute the NLO transverse momentum differential cross section of Z the boson. The result will show explicitly the appearance of logarithmic divergences in the semi-inclusive cross section, which is the main problem to be solved in the next two chapters.

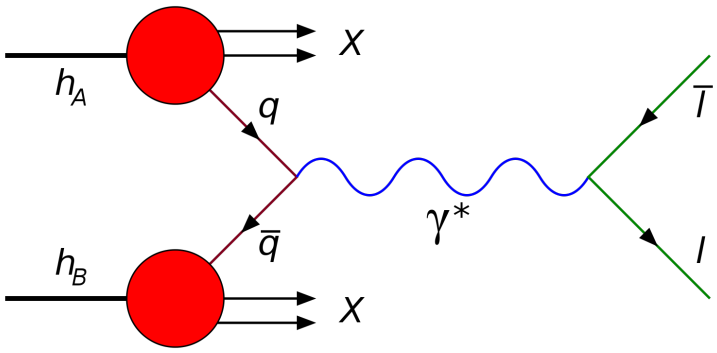

Figure 2: Drell Yan process in the parton model. The hard process in this figure is at leading order (LO) with γ being the intermediate state.

2.1 Drell Yan Mechanism

The mechanism of Drell Yan process is denoted as

$$\begin{aligned} h_1(p_{\rm A}) + h_2(p_{\rm B}) &\rightarrow q(p_1) + \bar{q}(p_2) + X_1 \\ &\rightarrow \gamma^*/Z/W(q) + X_2 \\ &\rightarrow l(k) + l'(k') + X_2, \end{aligned} \tag{15}$$

where ll' are l^+l^- for γ^* and Z, while are $l\nu$ for W. Momenta of the quark anti-quark pair are related to the hadron momenta as $p_1 = x_1 p_{\rm A}$, $p_2 = x_2 p_{\rm B}$. The decay of electroweak bosons into lepton pairs is purely electroweak process and the momentum is conserved as $q = k + k'$. Invariant mass of the lepton pair is defined as $Q^2 = (k + k')^2$, which is an important variable measured by experiments. Q^2 is also the virtuality of the vector bosons as $Q^2 = q^2$ and $Q^2 > 0$ since the vector bosons are timelike.

A typical scaling factor for Drell Yan process is $\tau = Q^2/s$, where $s = (p_{\rm A} + p_{\rm B})^2$ is the Mandelstam variable. Another important variable is called rapidity and is defined as

$$y \equiv \frac{1}{2}\ln\left(\frac{q \cdot p_{\rm A}}{q \cdot p_{\rm B}}\right). \tag{16}$$

Then the Bjorken scaling variables can be written as $x_1 = \frac{Q}{\sqrt{s}}e^y$, $x_2 = \frac{Q}{\sqrt{s}}e^{-y}$.

Since the decay rates of vector bosons are fairly small, the Drell Yan process can be regarded as the production of these effectively stable bosons multiplied by their branching ratios to different lepton pair final states.

The diagram for the process at Born level has been shown in Fig. 2. The total cross section of the Z production is [14]

$$\sigma^{(0)}_{q\bar{q}\to Z} = \frac{\pi}{3}\sqrt{2}G_{\rm F}M_{\rm Z}^2(V_q^2 + A_q^2)\delta(\hat{s} - Q^2), \tag{17}$$

where $\hat{s} \equiv (p_1 + p_2)^2 = x_1 x_2 s$.

2.2 Factorization of Drell Yan Process

Factorization theory of perturbative QCD is the field theory version and generalization of parton model. It is firstly used in the deep elastic scattering (DIS) process [10]. And it has been proved to be a general feature of the hard processes in QCD [15]. The basic idea of factorization is to absorb all the collinear and soft divergences arising in the QCD hard processes into the PDF's. One can do this since IR divergences will cancel with each other when all the divergent diagrams have been added into the inclusive cross section. The PDF's derived in this way will depend on an energy scale $\mu_{\rm F}$, which is called the factorization scale. The PDF will evolve with respect to this scale and the evolution equations are derived from the convolution of contributions from different divergent diagrams.

The next leading order contributions at $\mathcal{O}(\alpha_{\rm s})$ for the Drell Yan process include all the diagrams shown in Fig. 3. Soft divergences are given by the zero-mass of gluons in all the next-to-leading diagrams. Collinear divergences are given by the splitting of initial states shown in Fig. 3(b) and Fig. 3(c).

According to the first order factorization theorem for Drell Yan process, the collinear divergences will be cancelled when all the diagrams at this order are added. The contributions all together give rise to the scale dependent parton distributions $f_{a/h}(x, \mu_{\rm F}^2)$. The explicit formula of the scale dependent PDF's depend on different factorization schemes, in which singularities are absorbed in different ways. Based on this, the inclusive cross section should be written as

$$d\sigma^{\rm V}_{\rm h_1 h_2} = \Sigma_{ab}\int_0^1 dx_1 \int_0^1 dx_2 f_{a/h_1}(x_1, \mu_{\rm F}^2) f_{b/h_2}(x_2, \mu_{\rm F}^2)\hat{\sigma}^{\rm V}_{ab}, \tag{18}$$

instead of the original parton model formula in Eq. (14).

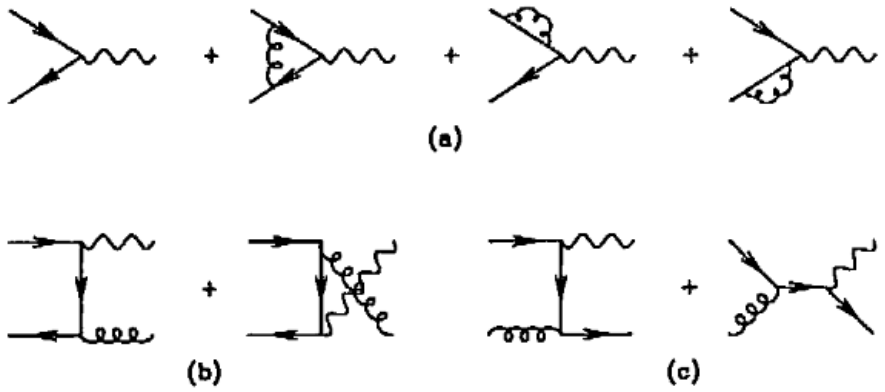

Figure 3: Leading order and next leading order diagrams for Drell Yan process [23].

Evolution equations of PDF's with respect to the factorization scale are called Dokshitzer-Gribov-Lipatov-Altarelli-Parisi evolution equations (DGLAP) [16, 17]. The differential equations are

$$\mu^2 \frac{df_{a/h}(x,\mu^2)}{d\mu^2} = \sum_b \int_x^1 \frac{d\xi}{\xi} P_{ab}\big(\frac{x}{\xi}, \alpha_{\rm s}(\mu^2)\big) f_{b/h}(\xi,\mu^2), \tag{19}$$

where $P_{ab}(\frac{x}{\xi}, \alpha_{\rm s}(\mu^2))$ is the evolution kernel and can be expanded and calculated perturbatively.

2.3 Transverse Momentum Distribution

There are two sources of vector bosons' non-zero transverse momentum $q_{\rm T}$ for Drell Yan processes. Firstly, transverse momentum of partons confined in the initial hadrons, which is called intrinsic transverse momentum, can give non-zero $q_{\rm T}$ to vector bosons. This effect is non-perturbative and thus only manifested in the kinematic region of $Q^2 \gg q_{\rm T}^2 \sim \Lambda_{\rm QCD}^2$. It can be easily described by a Gaussian-type intrinsic $q_{\rm T}$ distribution [14], or by a more complex formalism called transverse momentum dependent (TMD) factorization of QCD [23, 24], which is an updated version the factorization formula Eq. (18).

Another source of $q_{\rm T}$ is the QCD correction of hard processes, for example the NLO diagrams shown in Fig. 4. Such corrections can give large

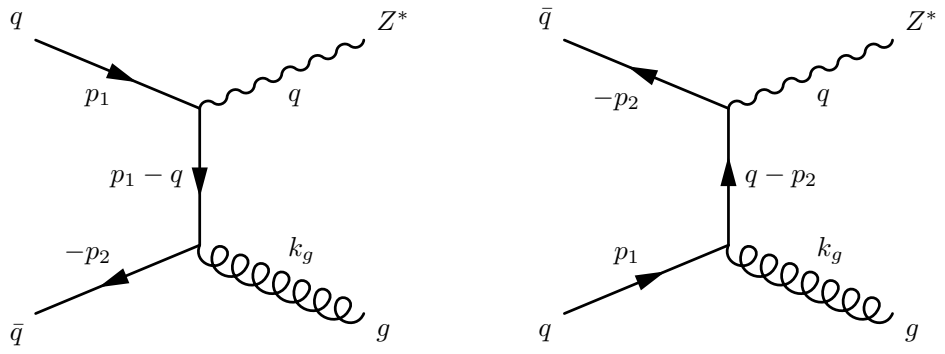

Figure 4: NLO corrections to $q\bar{q} \to Z$: real emission of gluons

q_{T} to the produced vector bosons. However, fixed order calculation of these corrections will give logarithmic dependence to the differential cross section. The logarithmic dependence arises from the soft and collinear singularities of the hard process kinematics and will ruin the perturbative expansion as q_{T} becomes small. This problem can be solved by the summation of logarithmic contributions. Such a method is called transverse momentum resummation.

Fixed order QCD corrections to the transverse momentum distribution for Drell Yan process have been known up to the next-next-to-leading order (NNLO) accuracy [18, 19, 20]. We firstly calculate the NLO corrections to the transverse momentum differential cross section in this section, which will show the logarithmic dependence explicitly. And in the next chapter, discuss the resummation method with more details.

The real emission of gluons at NLO with Z boson as the intermediate state shown in Fig. 4 is a two-to-two scattering. In the center of mass (CM) frame

$$d\sigma_{q\bar{q}\to Zg} = \frac{1}{2E_q 2E_{\bar{q}}|v_q - v_{\bar{q}}|}\frac{1}{(2\pi)^2}|\mathcal{M}_{q\bar{q}\to Zg}|^2\frac{d^3p_{\mathrm{Z}}d^3p_{\mathrm{g}}}{2E_{p_{\mathrm{Z}}}2E_{p_{\mathrm{g}}}}\delta^{(4)}(p_q + p_{\bar{q}} - p_{\mathrm{Z}} - p_{\mathrm{g}}). \tag{20}$$

With the rapidity defined in Eq. (16), the four momentum of the Z boson can be written as

$$q = (m_{\mathrm{T}}\mathrm{cosh}y, \mathbf{q}_{\mathrm{T}}, m_{\mathrm{T}}\mathrm{sinh}y), \tag{21}$$

where $m_{\rm T}=\sqrt{q_{\rm T}^2+Q^2}$ is the transverse mass. Accordingly $d^3q=\pi q^0 dq_{\rm T}^2 dy$. Define new Mandelstam variables of the hard process:

$$\hat{s}=-(p_q+p_{\bar{q}})^2,\ \hat{u}=-(p_q-q)^2,\ \hat{t}=-(p_{\bar{q}}-q)^2. \tag{22}$$

According to Eq. (21) and Eq. (22),

$$\begin{aligned}\frac{d^3p_{\rm Z}}{2E_{p_{\rm Z}}}\cdot\frac{d^3p_{\rm g}}{2E_{p_{\rm g}}}&\delta^{(4)}(p_q+p_{\bar{q}}-p_{\rm Z}-p_{\rm g})\\ &=\frac{\pi^2}{4}dq_{\rm T}^2dy\cdot d\hat{u}d\hat{t}\cdot\delta(\hat{s}+\hat{u}+\hat{t}-Q^2)\delta(\hat{s}k_{\rm T}^2-\hat{u}\hat{t})\\ &=\frac{\pi^2}{4}dq_{\rm T}^2dQ^2\frac{d\hat{u}d\hat{t}}{\hat{u}-\hat{t}}\delta(\hat{s}+\hat{u}+\hat{t}-Q^2)\delta(\hat{s}k_{\rm T}^2-\hat{u}\hat{t}).\end{aligned} \tag{23}$$

Then the transverse momentum differential cross section reads

$$\frac{d\sigma_{q\bar{q}\to Zg}}{dQ^2dq_{\rm T}^2}=\frac{1}{32\hat{s}}\int|\mathcal{M}_{q\bar{q}\to Zg}|^2\delta(\hat{s}+\hat{u}+\hat{t}-Q^2)\delta(\hat{s}q_{\rm T}^2-\hat{u}\hat{t})\frac{d\hat{u}d\hat{t}}{\hat{u}-\hat{t}}. \tag{24}$$

Matrix elements of the real emissions are calculated according to the Feynman diagrams in Fig. 4. $|\mathcal{M}_{q\bar{q}\to Zg}|^2$ is the unpolarized and spin summed squared amplitude, say $|\mathcal{M}_{q\bar{q}\to Zg}|^2=|\mathcal{M}|^2/4$ where

$$i\mathcal{M}=\frac{-igg_{\rm W}}{2\cos\theta_{\rm W}}\varepsilon_\mu^*(q)\epsilon_\nu^*(k_g)\bar{v}(p_2)\left[\gamma^\nu\frac{1}{\not{p}_1-\not{q}}\gamma^\mu+\gamma^\mu\frac{1}{\not{p}_1-\not{k}_g}\gamma^\nu\right](V_{\rm q}-A_{\rm q}\gamma_5)u(p_1), \tag{25}$$

in which $V_u=\frac{1}{2}-\frac{4}{3}\sin^2\theta_{\rm w}$, $A_u=\frac{1}{2}$, $V_d=-\frac{1}{2}+\frac{2}{3}\sin^2\theta_{\rm w}$, $A_d=-\frac{1}{2}$ and $\sin^2\theta_{\rm w}=0.23126$ [21]. Then

$$\frac{1}{4}|\mathcal{M}|^2=\frac{g^2g_{\rm W}^2}{2\cos^2\theta_{\rm W}}(V_{\rm q}^2+A_{\rm q}^2)\Big\{\big[(1-\frac{\mu^2}{\hat{u}})(\frac{Q^2}{\hat{u}}-1)-\frac{\hat{s}}{\hat{u}}\big]+\big[(1-\frac{\mu^2}{\hat{t}})(\frac{Q^2}{\hat{t}}-1)-\frac{\hat{s}}{\hat{t}}\big]+2\frac{\hat{s}}{\hat{u}\hat{t}}(Q^2+\mu^2)\Big\} \tag{26}$$

where μ is the virtuality of gluons. Take $\mu=0$,

$$\frac{1}{4}|\mathcal{M}|^2=24\sigma_{q\bar{q}\to Z}^{(0)}\alpha_s\big(\frac{Q^4+\hat{s}^2}{\hat{u}\hat{t}}-2\big), \tag{27}$$

where $\sigma_{q\bar{q}\to Z}^{(0)}=\frac{\pi}{3}\sqrt{2}G_{\rm F}m_{\rm Z}^2(V_{\rm q}^2+A_{\rm q}^2)$ is the Born level total cross section for Drell Yan process.

Now plug the matrix element in Eq. (27) into Eq. (24) and integral over dQ^2, the transverse momentum differential cross section reads

$$\begin{aligned}\frac{d\sigma_{q\bar{q}\to Zg}}{dq_{\rm T}^2} =&\frac{3}{4}\sigma^{(0)}_{q\bar{q}\to Z}\cdot\alpha_s\int\frac{(\hat{s}+\hat{u})^2+(\hat{s}q_{\rm T}^2/\hat{u}+\hat{s})^2}{\hat{s}^2q_{\rm T}^2(\hat{u}-\hat{s}q_{\rm T}^2/\hat{u})}d\hat{u}\\ \equiv&\frac{3}{4}\sigma^{(0)}_{q\bar{q}\to Z}\cdot\mathcal{I}(q_{\rm T}^2,\alpha_{\rm s}).\end{aligned}\tag{28}$$

In the limit of $\hat{s}q_{\rm T}^2 \ll Q^2$,

$$\begin{aligned}\mathcal{I}(q_{\rm T}^2,\alpha_{\rm s}) \approx&\alpha_s\frac{2}{\hat{s}q_{\rm T}^2}\int_{q_{\rm T}^2}^{Q^2}\big[1+\frac{\hat{s}}{\hat{u}}+\frac{1}{2}\frac{\hat{u}}{\hat{s}}\big]d\hat{u}\\ =&\alpha_s\frac{2}{\hat{s}}\bigg[\frac{\hat{s}}{q_{\rm T}^2}\ln(\frac{Q^2}{q_{\rm T}^2})+\big(1+\frac{4\hat{s}}{Q^2}\big)\frac{Q^2}{q_{\rm T}^2}-1-\frac{q_{\rm T}^2}{4\hat{s}}\bigg].\end{aligned}\tag{29}$$

Fig. 5 is the $q_{\rm T}$ distribution prediction with leading QCD real emissions at $E = 14$TeV hadron collider calculated according to the above formula.

The feynman diagram of the leading order virtual corrections is shown in Fig. 6. The matrix element is accordingly

$$\begin{aligned}i\mathcal{M}^{\rm V} =&\frac{\alpha_{\rm s}}{2\pi}\int_0^1 dx\int_0^{1-x}dz\big[\log\big(\frac{z\mu^2}{z\mu^2-x(1-x-z)q^2}\big)+\frac{(1-x)(x+z)q^2}{z\mu^2-x(1-x-z)q^2}\big]\\ &(\frac{-ig_{\rm W}}{2\cos\theta_{\rm W}})\varepsilon^*_\mu(q)\bar{v}(p_2)\gamma^\mu(V_{\rm q}-A_{\rm q}\gamma_5)u(p_1)\end{aligned}\tag{30}$$

where $\Delta = z\mu^2-x(1-x-z)q^2-z(1-z)p_1^2$. The amputation of the external legs have been considered. Write

$$F(Q^2,\alpha_{\rm s}) = \frac{\alpha_{\rm s}}{2\pi}\int_0^1 dx\int_0^{1-x}dz\big[\log\big(\frac{z\mu^2}{z\mu^2-x(1-x-z)q^2}\big)+\frac{(1-x)(x+z)q^2}{z\mu^2-x(1-x-z)q^2}\big],\tag{31}$$

then the function $F(Q^2,\alpha_{\rm s})$ can be regarded as QCD correction to the electroweak coupling constant. Up to the first order of g^2, i.e. α_s, the unpolarized and spin summed squared amplitude is

$$\frac{1}{3}|\mathcal{M}^{\rm V}|^2 = F(Q^2,\alpha_{\rm s})\cdot\frac{4}{\pi}\hat{s}\sigma^{(0)}_{q\bar{q}\to Z}.\tag{32}$$

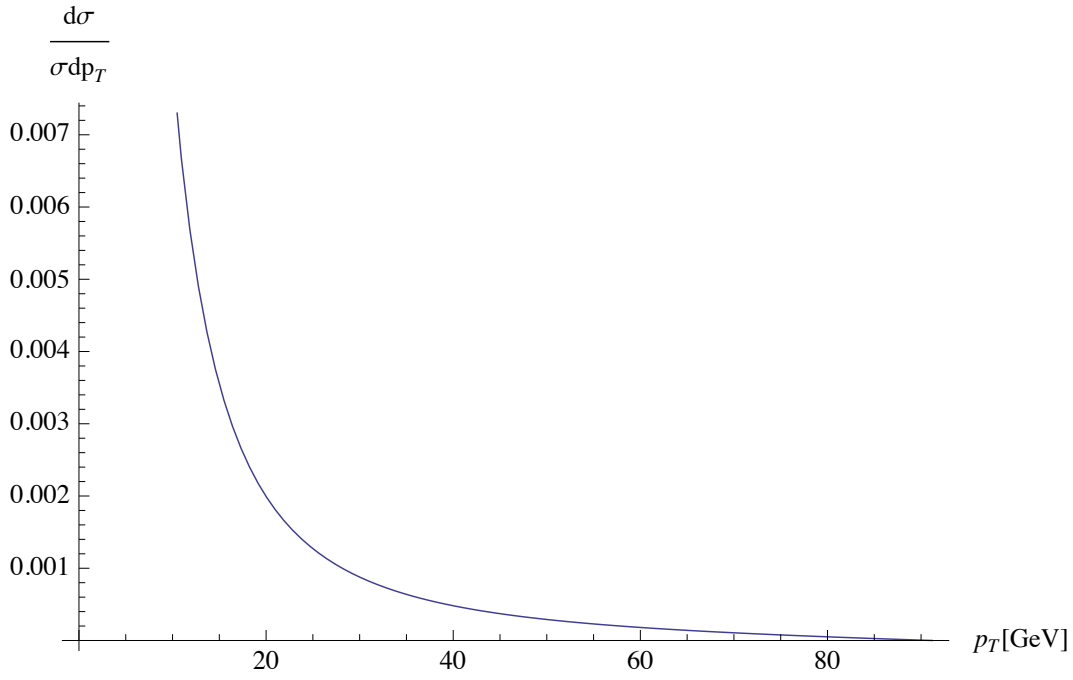

Figure 5: NLO q_{T} distribution of $q\bar{q} \to Z$ at 14TeV

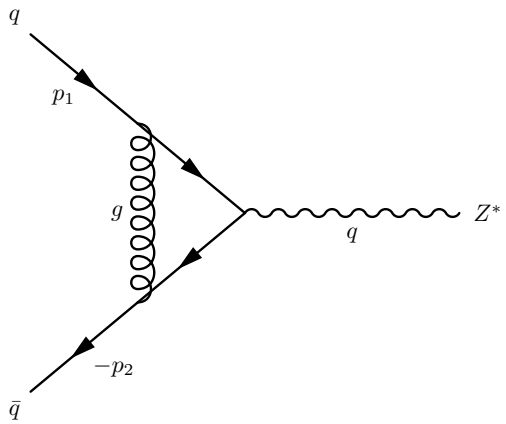

Figure 6: NLO corrections to $q\bar{q} \to Z$: virtual gluons

Using the relation $d^3q = \pi q^0 dq_{\rm T}^2 dy$, where y is the rapidity of Z boson, the differential cross section of the virtual correction is

$$\begin{aligned}\frac{d\sigma^{\rm V}}{dq_{\rm T}^2} =&\frac{\pi}{4\hat{s}}\int\frac{1}{3}|\mathcal{M}^{\rm V}|^2\delta(m_{\rm T}e^{y}-Ex_1)\delta(m_{\rm T}e^{-y}-Ex_2)\delta(q_{\rm T}^2)dy\\ =&\sigma^{(0)}_{q\bar{q}\to Z}F(Q^2,\alpha_{\rm s})\delta(q_{\rm T}^2)\delta(Q^2-\hat{s}).\end{aligned} \tag{33}$$

Divergence of the function $F(Q^2,\alpha_{\rm s})$ in the limit $\mu\to 0$ occurs when $z\approx 1,\ x\approx 0$. Near such a divergent region, the dominant part of $F(Q^2,\alpha_{\rm s})$ is then [22]

$$\begin{aligned}F(Q^2,\alpha_{\rm s}) \approx&\frac{\alpha_{\rm s}}{2\pi}\int_0^1 dx\int_0^{1-x}dz\frac{q^2}{\mu^2-x(1-x-z)q^2}\\ =&\frac{\alpha_{\rm s}}{2\pi}\int_0^1 dx\int_0^1 d\xi\frac{(1-x)q^2}{\mu^2-x(1-x)(1-\xi)q^2}\\ \approx&\frac{\alpha_{\rm s}}{2\pi}\int_0^1 dx\int_0^1 d\xi\frac{q^2}{\mu^2-x(1-\xi)q^2}\\ =&-\frac{\alpha_{\rm s}}{2\pi}\int_0^1 dx\Big[\frac{1}{x}\ln\frac{1}{x}+\frac{1}{x}\ln\frac{\mu^2}{Q^2}\Big].\end{aligned} \tag{34}$$

Summing over the real and virtual contributions, the total transverse momentum distribution at NLO, i.e. up to the first order of $\alpha_{\rm s}$, for Drell Yan process is then

$$\frac{d(\sigma^{\rm V}+\sigma^{\rm R})}{dq_{\rm T}^2} = \sigma^{(0)}_{q\bar{q}\to Z}\Big[\frac{3}{4}\mathcal{I}(Q^2,\alpha_{\rm s})+F(Q^2,\alpha_{\rm s})\delta(Q^2-\hat{s})\delta(q_{\rm T}^2)\Big]. \tag{35}$$

In the region of $q_{\rm T}^2\sim Q^2$, the virtual correction gives no contribution due to the delta function $\delta(q_{\rm T}^2)$. Thus in this region,

$$\frac{d(\sigma^{\rm V}+\sigma^{\rm R})}{dq_{\rm T}^2}\Big|_{\text{high } q_{\rm T}} = \frac{3}{4}\sigma^{(0)}_{q\bar{q}\to Z}\mathcal{I}(Q^2,\alpha_{\rm s}). \tag{36}$$

However in the region of $q_{\rm T}^2\ll Q^2$, the delta function contributes and then

the total contribution is approximately

$$\begin{aligned}
\frac{d(\sigma^{\rm V}+\sigma^{\rm R})}{dq_{\rm T}^2}\Big|_{\text{low } q_{\rm T}} &\approx \sigma^{(0)}_{q\bar{q}\to Z}\frac{3\alpha_{\rm s}}{2\hat{s}}\Big[\frac{\hat{s}}{q_{\rm T}^2}\ln(\frac{Q^2}{k_{\rm T}^2})+\big(1+\frac{4\hat{s}}{Q^2}\big)\frac{Q^2}{q_{\rm T}^2}-1-\frac{q_{\rm T}^2}{4\hat{s}} \\
&\qquad -\frac{\hat{s}}{3\pi}\delta(Q^2-\hat{s})\delta(q_{\rm T}^2)\int_0^1 dx\big(\frac{1}{x}\ln\frac{1}{x}+\frac{1}{x}\ln\frac{\mu^2}{Q^2}\big)\Big] \\
&= \sigma^{(0)}_{q\bar{q}\to Z}\frac{3\alpha_{\rm s}}{2Q^2}\Big[\frac{Q^2}{q_{\rm T}^2}\ln(\frac{Q^2}{q_{\rm T}^2})+5\frac{Q^2}{q_{\rm T}^2}-1-\frac{q_{\rm T}^2}{4Q^2} \\
&\qquad -\frac{1}{3\pi}\delta(\frac{q_{\rm T}^2}{Q^2})\int_0^1 dx\big(\frac{1}{x}\ln\frac{1}{x}+\frac{1}{x}\ln\frac{\mu^2}{Q^2}\big)\delta(Q^2-\hat{s})\Big] \\
&= \sigma^{(0)}_{q\bar{q}\to Z}\frac{3\alpha_{\rm s}}{2Q^2}\bigg(\big[\frac{Q^2}{q_{\rm T}^2}\ln\frac{Q^2}{q_{\rm T}^2}\big]_+ +5\big[\frac{Q^2}{q_{\rm T}^2}\big]_+ -1-\frac{q_{\rm T}^2}{4Q^2}\bigg),
\end{aligned} \tag{37}$$

where the plus distribution for a function $f(x)$ with a singular point at 0 is defined as

$$f(x)_+ = f(x)-\delta(x)\int_0^1 f(y)dy. \tag{38}$$

Such a plus distribution will give a finite result when integral over $q_{\rm T}^2$.

Chapter 3 Transverse Momentum Resummation

According to the fixed order calculation in the last chapter, logarithmic terms arise in the transverse momentum differential cross section for Drell Yan process. More explicitly, each perturbative term of the differential cross section for DY process will always be proportional to $\alpha_s^N \ln(Q^2/q_{\rm T}^2)^n$ with $n = N+1, ..., 2N-1$, which makes the perturbative expansion invalid in the region of very small $q_{\rm T}$. This is a common problem shared by all QCD hard processes with high Q. Transverse momentum resummation can solve the problem by summing over logarithmic contributions into an exponentially form factor, which is non-singular as $q_{\rm T} \to 0$.

Resummation is firstly proposed in [25], where only the leading logarithmic contribution, i.e. terms of the type $\alpha_s^N (\ln M^2/p_{\rm T}^2)^{2N-1}$ for a specific perturbative order N, is summed over. Such an approximation is called double-leading-logarithm approximation (DLLA) and the resummation formula is called DDT formalism.

To sum over logarithms to higher levels, it is convenient to do the resummation in b-space, which is the Fourier conjugate space of $q_{\rm T}$ and called the impact parameter space.

A complete resummation formalism, which can resum all orders of logarithms, is given by [29]. The formalism used the back-to-back jets technique developed earlier [30].

One problem with the formalism in [30] is that the Sudakov form factor is not universal for different processes. The formalism proposed in [35, 36] separates the part which is universal for all processes and the process-dependent part.

In this chapter, we firstly describe briefly the DDT's formalism and the approach used by Collins and Soper. Then we discuss the pros and cons of resummation in $q_{\rm T}$-space and b-space. Finally, we give the formalism in [35], which is the formula we are going to use in the calculation in Chapter 5.

3.1 DDT Formula

The leading logarithmic approximation (LLA) made in the DDT formulism of transverse momentum resummation [25] is in the kinematic region of

$$\frac{\alpha_{\rm s}(\mu^2)}{\pi} \ll 1, \ \frac{\alpha_{\rm s}(\mu^2)}{\pi} \ln \frac{q_{\rm T}^2}{\mu^2} \sim 1, \tag{39}$$

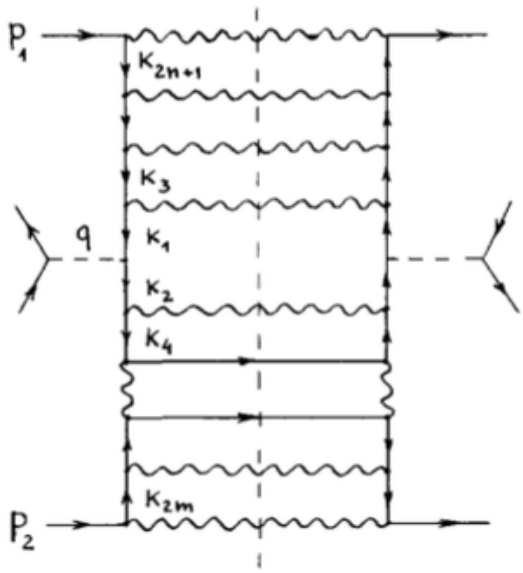

Figure 7: Ladder structure of the soft and collinear emissions for Drell Yan Process

where μ is the soft scale of the process. In this case, within all the logarithmic terms $(\alpha_s/\pi)^N \ln(Q^2/q_T^2)^n$ with $n = N+1, ..., 2N-1$ for a fixed order N, only the term $(\alpha_s/\pi)^N \ln(Q^2/q_T^2)^{2N-1}$ will give large contributions at very small q_T. Accordingly, other terms can be neglected based on the perturbative argument and only the leading logarithmic term needs to be resummed.

The planar gauge is used in the DDT's formula. Under planar gauge, the gluon propagator is

$$G_{\mu\nu} = \frac{d_{\mu\nu}(k)}{k^2 + i\epsilon},\ d_{\mu\nu}(k) = g_{\mu\nu} - \frac{k_\mu c_\nu + k_\nu c_\mu}{k \cdot c}, \tag{40}$$

where

$$c_\mu = Aq_\mu + Bp_\mu,\ A/B \approx 1, \tag{41}$$

with p and q defined in Eq. (12). It is proved that using planar gauge, leading logarithmic terms of the type $(\alpha_s/\pi)^N \ln(Q^2/q_T^2)^{2N-1}$ originate from the highly ordered kinematic structure of soft and collinear emissions.

Introduce Sudakov variables α_i and β_i of the emission process

$$k_{i\mu} = \alpha_i p_{1\mu} + \beta_i p_{2\mu} + k_{i\mathrm{T}\mu}, \tag{42}$$

where p_1 and p_2 are momenta of the colliding partons, k_i is momentum of the i'th emitted parton and $k_{i\mathrm{T}}$ is its transverse component. Then the highly ordered kinematic structure is parametrized as

$$\begin{aligned} &1 \geq ...\alpha_{2n+1} \geq ... \geq \alpha_1 = x_1, \\ &1 \geq ...\beta_{2m} \geq ... \geq \beta_2 = x_2. \end{aligned} \tag{43}$$

Such a phase space corresponds to the ladder structure of the Feynman diagrams for squared matrix elements. Fig. 7 is a typical ladder diagram for Drell Yan process.

Based on the highly ordered structure, the integration over phase space can be fully factorized. And the ladder diagrams can be calculated easily with such factorized integration. Summing over contributions from these ladder diagrams, the leading logarithmic terms are resummed into an exponential Sudakov form factor. The partonic differential cross section given by DDT formalism is finally

$$\frac{d\sigma}{dq_{\mathrm{T}}^2} = \sigma^{(0)} C_F \frac{\alpha_s}{\pi} \frac{\ln(\hat{s}/q_{\mathrm{T}}^2)}{q_{\mathrm{T}}^2} \exp\big(- C_F \frac{\alpha_s}{2\pi} \ln^2 \frac{\hat{s}}{q_{\mathrm{T}}^2} \big) \delta(\hat{s} - Q^2). \tag{44}$$

To fully factorize the highly ordered phase space, several other approximations are made in DDT formalism [26]. Firstly, the non-trivial energy conservation and transverse momentum conservation constraints on the phase space are ignored. Secondly, although the upper limits of Sudakov variables depend on $\hat{s}$ and q_{T}^2 explicitly, they are all set to be 1 to simplify the calculation. To give higher accuracy of the resummation, these approximations need to be released. The b-space resummation proposed in [27, 28] can solve the problem of transverse momentum conservation and give better kinematics. Also, because of the existence of a saddle point $b_\star$ in b-space resummation formalism, the behavior at the point of $q_{\mathrm{T}} \simeq 0$ is controlled by the saddle point and thus is computable [27] for very large Q.

3.2 Resummation from Back-to-back Jets

The DDT formalism can only resum the leading logarithmic contributions. Several modifications and developments are made afterwards. The most

complete formalism, which can resum all orders of logarithms, is given by [29]. The formalism is based on the the back-to-back jets technique developed earlier [30].

Contributions from large and small $q_{\rm T}$ are separated in [29]. The dominant contribution at small $q_{\rm T}$ region needs to be resummed while the other part is only important when $q_{\rm T} \sim Q$. The total differential cross section then has the general formula as

$$\frac{d\sigma}{dQ^2 dq_{\rm T}^2 dy} \sim \frac{4\pi^2\alpha^2}{9Q^2 s}\left\{(2\pi)^{-2}\int d^2b e^{i\mathbf{q}_{\rm T}\cdot\mathbf{b}}\tilde{W}(b;Q,x_A,x_B)+Y(q_{\rm T};Q,x_A,x_B)\right\}, \tag{45}$$

where x_A and x_B are Bjorken variables of the colliding hadrons A and B. The first term is the resummation part, which is calculated in the b-space. The second term is the large $q_{\rm T}$ part, which contains no logarithmic contribution and can be neglected in the small $q_{\rm T}$ region.

The large $q_{\rm T}$ contribution $Y(q_{\rm T};Q,x_A,x_B)$ is extracted from regular part of the the factorization formula

$$\frac{d\sigma}{dQ^2 dq_{\rm T}^2 dy} = \frac{4\pi^2\alpha^2}{9Q^2 s}\sum_{a,b}\int_{x_A}^1 \frac{d\xi_A}{\xi_A}\int_{x_B}^1 \frac{d\xi_B}{\xi_B} f_{a/A}(\xi_A;\mu_{\rm F}^2) f_{b/B}(\xi_B;\mu_{\rm F}^2)$$
$$T_{ab}(q_{\rm T},Q;x_A/\xi_A,x_B/\xi_B;\alpha_{\rm s}(\mu_{\rm F}^2),\mu_{\rm F}), \tag{46}$$

which is valid with $q_{\rm T}$ integrated or in the large $q_{\rm T}$ region. One trick is that the variable $q_{\rm T}$ in the explicit expression of Y is replaced by $[q_{\rm T}^2+(q_{\rm T}^{\rm min})^2]^{1/2}$ to cut off certain weak singularities as $q_{\rm T}\to 0$. $q_{\rm T}^{\rm min}$ is chosen to be a small non-zero value.

Matching between small and large $q_{\rm T}$ contributions is needed. The matching is implemented as follows. Firstly in the large $q_{\rm T}$ region, the resummed part $\tilde{W}$ will have the ordinary factorization formula but only its singular part. Then $\tilde{W}$ and Y together will give rise to the total factorization result. While in the small $q_{\rm T}$ region, contribution from Y is negligible compared to $\tilde{W}$ and then the resummation formula of $\tilde{W}$ alone is required to be a good approximation to the cross section.

The formula for $\tilde{W}$ is derived separately in the b-space region $b \ll 1/\Lambda$ and $b \geq 1/\Lambda$. Then the two parts are joined together based on an evolution equation of $\tilde{W}$ with respect to Q^2.

When $b \ll 1/\Lambda$, which corresponds to the large $q_{\rm T}$ region, $\tilde{W}$ is given by singular part of the factorization formula (46). Moreover, $\tilde{W}$ obeys an evo-

lution equation due to its convolution with PDF's. The differential equation is

$$\frac{\partial}{\partial \ln Q^2}\tilde{W}(b;Q,x_A,x_B) = -\left[\int_{C_1^2/b^2}^{C_2^2Q^2}\frac{d\bar{\mu}^2}{\bar{\mu}^2}A(\alpha_{\rm s}(\bar{\mu});C_1) + B(\alpha_{\rm s}(C_2Q);C_1,C_2)\right] \times \tilde{W}(b;Q,x_A,x_B), \tag{47}$$

where C_1 and C_2 are dimensionless variables. According to this evolution equation and the singular part of the factorization formula, $\tilde{W}$ has a general form

$$\begin{aligned}\tilde{W}(b;Q,x_A,x_B) =& \sum_{a,b}\int_{x_A}^1\frac{d\xi_A}{\xi_A}\int_{x_B}^1\frac{d\xi_B}{\xi_B}f_{a/A}(\xi_A;\mu_{\rm F}^2)f_{b/B}(\xi_B;\mu_{\rm F}) \\ &\times \exp\Big\{-\int_{C_1^2/b^2}^{C_2^2Q^2}\frac{d\bar{\mu}^2}{\bar{\mu}^2}\big[\ln(C_2^2Q^2/\bar{\mu}^2)A(\alpha_{\rm s}(\bar{\mu});C_1) + B(\alpha_{\rm s}(C_2Q);C_1,C_2)\big]\Big\} \\ &\times \sum_j e_j^2 C_{ja}(x_A/\xi_A,b;Qb,\alpha_{\rm s}(\mu_{\rm F}),\mu_{\rm F})C_{jb}(x_B/\xi_B,b;Qb;\alpha_{\rm s}(\mu_{\rm F}),\mu_{\rm F}),\end{aligned} \tag{48}$$

where the exponential term is the Sudakov form factor and the C_{ia}'s are coefficient functions. Factors $A(\alpha_{\rm s}(\bar{\mu});C_1)$, $B(\alpha_{\rm s}(C_2Q);C_1,C_2)$ and coefficients $C_{ja}(x_A/\xi_A,b;Qb,\alpha_{\rm s}(\mu_{\rm F}),\mu_{\rm F})$ can all be expanded perturbatively over $\alpha_{\rm s}$. The inclusion of different perturbative orders corresponds to different levels of logarithmic resummation.

In the region of $b \geq 1/\Lambda$, $\tilde{W}$ obeys the same evolution equation. But now the factors A and B also depend on quark masses. Moreover, extra constants will arise when doing integration of the evolution equation. But it has been prove that when Q is large enough, the integration over b in Eq. (45) is dominated by contributions from small b. There is a saddle point b_* for $\tilde{W}$ as the function of b. The integration is then dominated by such a saddle point. For example, if only including leading term of the factors A and B in Eq. (48), the saddle point is

$$b_* = \frac{1}{\Lambda}\Big(\frac{Q}{\Lambda}\Big)^{-A^{(1)}/[A^{(1)}+\beta_1]} \approx \frac{1}{\Lambda}\Big(\frac{Q}{\Lambda}\Big)^{-0.41}, \tag{49}$$

where $A^{(1)}$ is the first order coefficient of A and β_1 is the first order β-function. Then if Q is large enough, b_* will be much smaller than $1/\Lambda$, in which case the contribution from large b can be neglected.

One advantage of performing resummation in b-space is the existence of such a saddle point. In the $q_{\rm T}$ resummation formula, the point $q_{\rm T} = 0$ is singular and not calculable. However, in b-space, the point of $q_{\rm T} = 0$ corresponds to large b region. Then the point of $q_{\rm T} = 0$ can be calculated based on such a saddle point argument. Also, as is stated above, the Fourier transformation naturally give the conservation of transverse momentum. Thus the b-space resummation gives better kinematics.

However, there are also several disadvantages to perform resummation in the b-space. Firstly, the differential cross section is separated into two parts, which account for the behavior in low $q_{\rm T}$ and high $q_{\rm T}$ region respectively. Thus one in fact needs to use the resummation formalism in low $q_{\rm T}$ region, the fixed order calculation in high $q_{\rm T}$ region, and in the intermediate region, perform a matching procedure between the fixed order and resummation to give the exact result. On the other hand, some $q_{\rm T}$-space resummation can give unified formula valid for the whole kinematic region [31]. Moreover, while in the $q_{\rm T}$-space resummation, non-perturbative effects are only manifested at very low $q_{\rm T}$, the b-space resummation formalism needs to include non-perturbative effects in the whole b space, as it is the Fourier transformed space of $q_{\rm T}$.

3.3 A formalism with Universal Form Factor

Both form factor and coefficient function of the resummation formalism in Eq. (48) are in fact process dependent [33, 34], although the form factor is usually supposed to be or regarded to be universal. A new formalism proposed in [34, 35] separates the part which is universal for all processes and the process-dependent part and finally give a more concrete way to do the resummation.

As usual, the differential cross section is written in the factorization formula Eq. (18) and the partonic cross section is divided into the resummation part and finite part

$$\frac{d\hat{\sigma}^{\rm F}_{ab}}{dq^2_{\rm T}} = \left[\frac{d\hat{\sigma}^{\rm F,(res.)}_{ab}}{dq^2_{\rm T}}\right]_{\rm l.a.} + \left[\frac{d\hat{\sigma}^{\rm F,(fin.)}_{ab}}{dq^2_{\rm T}}\right]_{\rm f.o}, \tag{50}$$

where the subscript l.a. and f.o. denotes that the resummation and finite part calculation is done at fixed logarithmic accuracy (LL, NLL for example) and fixed perturbative order respectively in practice.

Since the finite part does not contain logarithmic divergent contributions, the way used in [35] to obtain the finite part is by subtracting resummation component from the total fixed order differential cross section. Then

$$\left[\frac{d\hat{\sigma}_{ab}^{\mathrm{F},(\mathrm{fin.})}}{dq_{\mathrm{T}}^2}\right]_{\mathrm{f.o}} = \left[\frac{d\hat{\sigma}_{ab}^{\mathrm{F}}}{dq_{\mathrm{T}}^2}\right]_{\mathrm{f.o}} - \left[\frac{d\hat{\sigma}_{ab}^{\mathrm{F},(\mathrm{res.})}}{dq_{\mathrm{T}}^2}\right]_{\mathrm{f.o}}, \tag{51}$$

where the resummation component at a fixed order is given by identifying terms of fixed order α_{s} in the resummation results. Explicit expressions of $[d\hat{\sigma}_{ab}^{\mathrm{F},(\mathrm{res.})}/dq_{\mathrm{T}}^2]_{\mathrm{f.o}}$ can be found in ref. [35]. There's one more constraint set to the finite part, say

$$\lim_{Q_{\mathrm{T}}\to 0}\int_0^{Q_{\mathrm{T}}^2} dq_{\mathrm{T}}^2\left[\frac{d\hat{\sigma}_{ab}^{\mathrm{F}}}{dq_{\mathrm{T}}^2}\right]_{\mathrm{f.o}} = 0. \tag{52}$$

This constraint ensures that the perturbative contribution proportional to $\delta(q_{\mathrm{T}}^2)$ has been excluded from the finite part. This is required to avoid double counting since the resummation part includes the delta contribution.

The resummation is done in the impact parameter space and the resummation partonic cross section is accordingly written as (subscript l.a. is understood)

$$\frac{d\hat{\sigma}_{ab}^{\mathrm{F},(\mathrm{res.})}}{dq_{\mathrm{T}}^2}(q_{\mathrm{T}}, Q, \hat{s}; \alpha_{\mathrm{s}}, \mu_{\mathrm{R}}^2, \mu_{\mathrm{F}}^2) = \frac{Q^2}{\hat{s}}\int_0^\infty db\frac{b}{2}J_0(bq_{\mathrm{T}})\mathcal{W}_{ab}^{\mathrm{F}}(b, Q, \hat{s}; \alpha_s, \mu_{\mathrm{R}}^2, \mu_{\mathrm{F}}^2), \tag{53}$$

where $\alpha_{\mathrm{s}} \equiv \alpha_{\mathrm{s}}(\mu_{\mathrm{R}}^2)$, $J_0(x)$ is the zeroth order Bessel function. The μ_{R} dependence of $d\hat{\sigma}_{ab}^{\mathrm{F},(\mathrm{res.})}/dq_{\mathrm{T}}$ comes from the running coupling while the μ_{F}^2 dependence comes from the factorization.

Define a new scaling factor $z = Q^2/\hat{s}$. Then it is convenient to perform the Mellin transform to transfer $\mathcal{W}_{ab}^{\mathrm{F}}$ from z-space into its conjugate N-space. Related factors are all written as functions of N later. The Mellin transformation is

$$\mathcal{W}_{ab,N}^{\mathrm{F}}(b, Q; \alpha_s, \mu_{\mathrm{R}}^2, \mu_{\mathrm{F}}^2) = \int_0^1 dz z^{N-1}\mathcal{W}_{ab}^{\mathrm{F}}(b, Q, Q^2/z; \alpha_s, \mu_{\mathrm{R}}^2, \mu_{\mathrm{F}}^2). \tag{54}$$

The N-components $\mathcal{W}_{ab}^{\mathrm{F}}$ has a general formula as

$$\begin{aligned}\mathcal{W}_{ab,N}^{\mathrm{F}}(b, Q; \alpha_s, \mu_{\mathrm{R}}^2, \mu_{\mathrm{F}}^2) = \sum_{\{\mathcal{I}\}}&\mathcal{H}_{ab,N}^{\mathrm{F},\{\mathrm{I}\}}(Q, \alpha_s; Q^2/\mu_{\mathrm{R}}^2, Q^2/\mu_{\mathrm{F}}^2, Q^2/M^2)\\ &\exp\left\{\mathcal{G}_N^{\{I\}}(\alpha_s, L; Q^2/\mu_{\mathrm{R}}^2, Q^2/M^2)\right\},\end{aligned} \tag{55}$$

where $L \equiv \ln\frac{M^2b^2}{b_0^2}$, $b_0 = 2e^{-\gamma_{\rm E}}$ and the sum over $\{I\}$ denotes summation over a series of indices. A new scale M is introduced to parametrize an arbitrariness arising from the factorizing between constant and logarithmic terms [40]. As is indicated by the superscript, function $\mathcal{G}_N^{\{I\}}$ is independent of the specific process F and the partonic channel ab while $\mathcal{H}_{ab,N}^{\rm F,\{I\}}$ is process dependent.

The form factor $\mathcal{G}_N^{\{I\}}$ in the general form (55) does the resummation of large logarithms, which is reflected by it's dependence on the variable L. It can be expanded perturbatively as

$$\begin{aligned}\mathcal{G}_N^{\{I\}}(\alpha_s, L; Q^2/\mu_{\rm R}^2, Q^2/M^2) =& Lg^{(1),\{c\}}(\alpha_s L) + g_N^{(2),\{c\}}(\alpha_s L; Q^2/\mu_{\rm R}^2, Q^2/M^2) \\ &+ \sum_{n=3}^{+\infty}\big(\frac{\alpha_{\rm s}}{\pi}\big)^{n-2} g_N^{(n),\{I\}}(\alpha_s L; Q^2/\mu_{\rm R}^2, Q^2/M^2).\end{aligned} \tag{56}$$

This form factor also has a formula similar to the Sudakov form factor S_c

$$\mathcal{G}_N^{\{I\}}(\alpha_s, L; Q^2/\mu_{\rm R}^2, Q^2/M^2) = -\int_{b_0^2/b^2}^{M^2}\frac{q^2}{dq^2}\big[A^{\{c\}}(\alpha_s(q^2))\ln\frac{Q^2}{q^2} + \tilde{B}_{N,\{I\}}(\alpha_s(q^2))\big], \tag{57}$$

where $A^{\{c\}}(\alpha_{\rm s})$ is the same as the factor $A(\alpha_{\rm s})$ of S_c in Eq. (48), however the coefficient $\tilde{B}_{N,\{I\}}(\alpha_s)$ is different from $B(\alpha_s)$ in the sense that it contains extra information of the PDF convolution. Accordingly, the explicit forms of $\tilde{B}_{N,\{I\}}(\alpha_s)$ can be derived from Sudakov form factors and parton anomalous dimensions. The perturbative coefficients $g_N^{(n),\{I\}}$'s in Eq. (56) are obtained from the perturbative expansion of factors in Eq. (57).

The newly introduced coefficient function $\mathcal{H}_{ab,N}^{\rm F,\{I\}}$ in Eq. (55) contains both the information of PDF convolution and all the process dependence which is extracted from the non-universal Sudakov form factor in the old form (48). It does not contain logarithmic terms and is independent of L accordingly. It is written perturbatively

$$\begin{aligned}&\mathcal{H}_{ab,N}^{\rm F,\{I\}}(Q, \alpha_s; Q^2/\mu_{\rm R}^2, Q^2/\mu_{\rm F}^2, Q^2/M^2) \\ &\quad= \sigma_{F\leftarrow\{c\bar{c}\}}^{(0)}(\alpha_s, Q)\bigg[1 + \frac{\alpha_{\rm s}}{\pi}\mathcal{H}_{N,\{c\bar{c}\}\leftarrow ab}^{(1)}(Q^2/\mu_{\rm R}^2, Q^2/\mu_{\rm F}^2, Q^2/M^2) \\ &\qquad+ \sum_{n=2}^{+\infty}\big(\frac{\alpha_{\rm s}}{\pi}\big)^n \mathcal{H}_{N,\{I\}\leftarrow ab}^{{\rm F},(n)}(Q^2/\mu_{\rm R}^2, Q^2/\mu_{\rm F}^2, Q^2/M^2)\bigg],\end{aligned} \tag{58}$$

where $\sigma^{(0)}_{F\leftarrow\{c\bar{c}\}}$ is the Born level partonic cross section of process $c\bar{c} \to F$.

To give kinematic corrections for large-$q_{\rm T}$, the variable L is replaced by $\tilde{L}$, which is defined as

$$\tilde{L} \equiv \ln(\frac{Q^2 b^2}{b_0^2} + 1). \tag{59}$$

In the region $Qb \gg 1$, i.e. $q_{\rm T} \ll Q$, $\tilde{L} = L + \mathcal{O}(1/(Qb))^2 \approx L$. Thus the replacement has no effect in this region. While when $Qb \ll 1$, i.e. the large $q_{\rm T}$ region, $\tilde{L} \to 0$ and then $\exp\{\mathcal{G}_N^{\{I\}}(\alpha_s, L)\} \to 1$, which means the logarithmic resummation effects are reduced.

There is a singularity in the resummation form factor $\mathcal{G}_N^{\{I\}}(\alpha_s, L)$, which is at the point of $\lambda \equiv \beta_0 \alpha_s L/\pi = 1$, i.e. $b^2 = (b_0^2/M^2)\exp(\pi/(\beta_0 \alpha_{\rm s}))$. This singularity originates from the divergence of running coupling $\alpha_{\rm s}(q^2)$ near the Landau pole. It is also the onset point of non-perturbative effects, after which the non-perturbative corrections need to be included. There are many prescriptions to regularize such singularities, one of which is the b_* prescription described in the last section. One can also extend the Fourier transformation of b into its complex plane and choose specific contour to avoid the pole. This is called 'minimal prescription' [38, 39]. We will describe this in more detail in chapter 5.

Chapter 4 Parton Shower Algorithms

Transverse momentum resummation can solve the problem of logarithmic divergence of semi-inclusive differential cross section for QCD processes. But it can only be applied to the calculation of differential cross sections. Another way to solve the problem is simulating a succession of soft and collinear QCD emissions from the incoming and outgoing partons of a process using Monte Carlo method. Such an algorithm is called a parton shower (PS).

A parton shower is mainly used in Monte Carlo event generators, like Herwig++ [51], Pythia 8 [52] and SHERPA [53], which is a general-purpose method to make QCD predictions for LHC. As is stated in the first chapter, there are both perturbative effects at short distance and non-perturbative effects at long distance of QCD. Thus the General Purpose Monte Carlo (GPMC) event generators have both approaches to long distance physics and short distance physics, for example the hadronization models and soft hadron-hadron models dealing with long distance QCD [54]. Parton shower is its main algorithm used for the short distance QCD.

This chapter is an introduction to basics of the parton shower algorithm.

4.1 Final State Radiation

As is stated in the resummation chapter, the leading contribution to the logarithmic divergence arising from the soft and collinear QCD emissions is the kinematic region where the hardness and/or angle of the radiation are highly ordered. The final state radiation (FSR) of parton shower is the simulation of such radiation from the final state partons.

Each splitting of FSR is labeled by the highly ordered measurable hardness or angle, which is parametrized as the order variable. Order variables can be either the virtuality of a parton, or the relative transverse momentum or angle between partons before and after the splitting. The virtuality of a parton is defined as

$$t = E^2 z(1-z)(1-\cos\theta) \approx z(1-z)E^2\frac{\theta^2}{2}, \tag{60}$$

where E is energy of the parton before splitting, z and $1-z$ are energy fractions carried by partons after splitting, θ is the relative angle. The relative angle is fairly small in the dominant collinear region. The relative transverse momentum is

$$q_{\mathrm{T}}^2 \approx z^2(1-z)^2E^2\theta^2 \tag{61}$$

in the small angle limit. It is easy to see that the strong ordering in these variables are all equivalent in the dominant region with small angle limit. However, there is a significant difference between the virtuality and transverse momentum being the ordering variable as z becoming small. Thus the differences between choices of ordering variables arises when radiation is soft but with large splitting angle, which is the next leading contribution to the logarithmic divergence.

Each intermediate line of the succession of soft and collinear emissions is associated with a factor. The final differential cross section for the process is obtained by multiplying the leading order differential cross section by all such factors. For example, use virtuality as the ordering variable, the factor for each intermediate line is

$$\Delta_i(t,t')\frac{\alpha_s(t)}{2\pi}P_{i,jk}(z)\frac{dt}{t}dz\frac{d\phi}{2\pi}, \tag{62}$$

where $P_{i,jk}(z)$ is the Altarelli-Parisi splitting function, i and jk corresponds to the incoming and outgoing partons respectively. $\Delta_i(t,t')$ is the familiar Sudakov form factor

$$\begin{aligned}\Delta_i(t,t') &= \exp\Big\{-\int_t^{t'}\frac{dq^2}{q^2}\frac{\alpha_s(q^2)}{2\pi}\int_{t/q^2}^{1-t/q^2}dz\sum_{jk}P_{i,jk}(z)\Big\}\\ &\sim \exp\Big\{-C_F\frac{\alpha_s}{2\pi}\ln^2\frac{t'}{t}\Big\},\end{aligned} \tag{63}$$

which corresponds to the DLLA or LL accuracy of the Sudakov form factor in resummation formalism. Thus the basic shower algorithm includes all the leading logarithmic corrections. The factor dt/t in Eq. (62) is the parametrization of phase space using order variable. If using the relative angle or transverse momentum as order variable, dt/t needs to be replaced by corresponding expressions according to the equivalent relation

$$\frac{dt}{t}=\frac{dq_{\rm T}^2}{q_{\rm T}^2}=\frac{d\theta^2}{\theta^2} \tag{64}$$

of ordering variables.

Throughout the evolution of FSR, the momentum, or the absolute value of virtuality, is transferred down from the hard scale to low scales like the factorization scale of partons. Ending of the splitting is also parametrized by the ordering variable, for example the infrared cutoff of virtuality t_0, which is defined by the shower hadronization scale or the width of an unstable particle.

4.2 Initial State Evolution

Incoming partons can also radiate before entering the hard process. Simulation of such QCD radiations is the initial state radiation (ISR) of parton shower. ISR can also give non-zero transverse momentum to partons but the corresponding virtuality is negative.

Different from FSR, ISR is base on a backwards-evolution algorithm [55]. The backward-evolution Sudakov form factor is

$$\Delta_i^{\mathrm{ISR}}(t,t') = \exp\Big\{ -\int_t^{t'} \frac{dq^2}{q^2}\frac{\alpha_s(q^2)}{2\pi}\int_x^1 \frac{dz}{z}\sum_{jk} P_{i,jk}(z)\frac{f_j(q^2,x/z)}{f_i(q^2,x)}\Big\}. \quad (65)$$

This is given by considering the ratio between PDF's before and after a splitting. Such evolution of PDF's can be controlled by the DGLAP equation introduced in chapter 2.

ISR also gives the leading logarithmic contribution, which is in the collinear dominant region. However in contrast to the FSR, the absolute value of virtuality is transferred from the low factorization scale up to the hard scale of the process.

4.3 Large Quark Mass Effects

In a parton shower, all partons are regarded as massless. But the non-zero quark masses can affect the shower algorithm by serving as cut off. When the quark mass is above the typical scale Λ_{QCD}, the splitting will end at quark mass scale rather than the hadronization scale.

For a quark with energy E and mass m, define the ratio $\theta_0 \equiv m/E$. Then using relative angle as ordering variable, parametrization of the phase space should be replaced as

$$\frac{d\theta^2}{\theta^2} \to \frac{\theta^2 d\theta^2}{(\theta^2+\theta_0^2)^2}. \quad (66)$$

Accordingly, the large angle radiation with $\theta \gg \theta_0$ won't be affected, while the collinear radiation with small angle will be largely suppressed. When $\theta \leq \theta_0$ the splitting is regulated and θ_0 becomes the cut-off of such radiations. This may happen before the hadronization scale cuts the virtuality ordering.

Such a feature can be implemented using the matrix element correction like in Pythia [56], or using a generalized Altarelli-Parisi splitting function for massive quarks like in Herwig++ and SHERPA [57].

Other aspects of parton showers are related to optimizing its logarithmic accuracy, which will be stated in the next chapter.

Chapter 5 Logarithmic Accuracy of Parton Shower Algorithms

According to the Sudakov form factor in Eq, (63), it is clear that FSR of parton shower only resums the leading logarithmic contributions arising from the soft and collinear emissions for hard processes of QCD. Also, the ISR is of leading logarithmic accuracy. However, there are several corrections within the parton shower algorithm or Monte Carlo event generator which can give higher level logarithmic resummation results.

In this chapter, we firstly analyze different approaches used by parton showers and Monte Carlo event generators to give higher resummation accuracy. Then the resummation prediction of transverse momentum distribution of Z boson for Drell Yan process is calculated. We use Pythia8 event generator to obtain the transverse momentum distribution prediction given by parton shower. Finally the numerical comparison between the parton shower prediction and the resummation logarithmic accuracy is made accordingly.

5.1 Higher Accuracy Logarithmic Resummation Approaches of Parton Shower

5.1.1 Soft Emissions and Coherence Effects

The first correction within the parton shower algorithm to give higher resummation accuracy is the inclusion of soft emissions. This approach treats the coherence problem of QCD bremsstrahlung and thus is called coherence effects. According to the analysis in [26], the LLA corresponds to soft and collinear partonic emissions, while the inclusion of hard collinear radiations and soft radiations with large transverse momentum will give the NLL accuracy. Moreover, amplitudes from different diagrams with soft wide-angle emissions have non-trivial phase structure and thus their interferences are no longer negligible, which are however neglected in the ladder structure of DLLA.

The coherence effects can be included in the parton shower algorithm by changing the ordering variable from virtuality t to relative angle θ between partons, say angular-ordering parton shower, like in HERWIG and HERWIG++ [41]. More specifically, the non-trivial coherence is the interference between wide range emission and collinear emissions. The contribution should be calculated as the amplitudes of diagrams with soft emissions attached to the the external partons. It is proved that the sum of all these kinds of diagrams equals to the configuration where the large angle emissions

Figure 8: Rules of the color flow construction in parton shower

happen before the collinear ones. Thus the ordering in relative angles can effectively approximate such interference.

Instead of using the relative angle as ordering variables, one can also impose an angular veto in virtuality-ordering parton shower to include such effects, like in the Pythia 6 [42] event generator.

5.1.2 Color Information and Dipole Approach

Another approach to parton shower, say the transverse-momentum-ordered dipole approach [43], which is used by some recent MC event generators like Pythia 8 [48], is equivalent to the coherence-improved parton showers described above.

The approach is based on color flow of the parton shower. The parton shower MC generators can track color information in the large-N_c limit, where the complicated parton system is decomposed as a color flow. Rules of the color flow construction are shown in Fig. 8. In the soft radiation and large-N_c limit, each of the lines in color flow emits independently, which is effectively an color-anticolor dipole. The collinear emissions can also be included into the color flow or dipole approach to the parton shower [49, 43]. It is implemented by modifying the rapidity distribution of the emitted gluons. Then either the collinear or soft radiations can be simulated. Thus the parton shower based on such an approach is believed to be able to reach the NLL accuracy.

5.1.3 Matching with ME and NLO

Another correction is made by matching between parton shower and fixed order prediction of the hard process. Overall, it will give higher logarithmic resummation accuracy to the MC event generator prediction.

Fixed order matrix elements can describe well-separated and hard partons while parton showers can only simulate soft and collinear partons. The total cross section given by the usual parton shower algorithm is only the Born

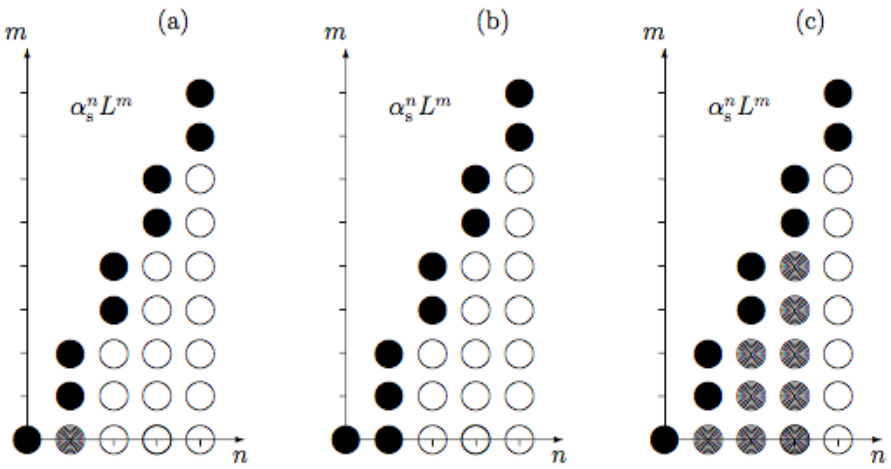

Figure 9: Logarithmic resummation accuracy of parton shower with ME/NLO corrections. (a) parton shower with ME matching. The blob is half-filled because that only real emission corrections are included; (b) parton shower with NLO matching (c) parton shower with multi-jets merging, where the half-filled blobs is due to that only real emissions above the merging scale are included.

level value. Thus, matching up the parton shower results with higher order matrix elements can optimize the simulation of the hard and large angle radiations.

The method has been done in the direction of the matching between PS and matrix elements, say PS+ME, and the matching between PS and next leading order calculation, say PS+NLO. The matrix element or NLO calculation gives inclusive quantities at a fixed perturbative order. While the parton shower generates exclusive states.

The PS+ME matching approach was first formulated in [44]. In the PS+ME method, the exact matrix elements with a certain number n of partons for the hard process are generated at first. The number of partons are below n and the relative transverse momentum of any pair of partons is above a cut-off scale $Q_{\rm cut}$ throughout the shower algorithm. Then the generated configuration is tree-level accurate at large angle and fits parton shower prediction at small angle radiations.

The PS+NLO method generates the process at NLO accuracy at first. Both the real emission correction and virtual correction at NLO are included. The NLO correction can be added simply by applying a constant K factor on the ME method, which will yield better prediction for $2 \to 1$ processes like the vector boson production if properly tuned. There are two main methods of PS+NLO, say MC@NLO [45] and POWHEG [46, 47].

In summary, Fig. 9 [50] shows the different logarithmic resummation accuracy to which different matching procedure can reach.

5.2 Transverse Momentum Distribution of Z Boson for Drell Yan Process: Resummation

We used the resummation formalism in section 3.3 to calculate the transverse momentum differential cross section of Z boson for Drell Yan process.

At the LL accuracy, there is no finite part correction. For the resummation part, the coefficient function $\mathcal{H}^{\rm F,\{I\}}_{ab,N}$ in Eq. (55) is just the Born level cross section and only the first order coefficient $g^{(1),\{c\}}(\alpha_s L) \equiv g_c^{(1)}(\alpha_s L)$ enters the form factor. Then the partonic differential cross section reads

$$\frac{d\hat{\sigma}^{\rm Z,LL}_{ab}}{dq_{\rm T}^2}(q_{\rm T}, Q, \hat{s}; \alpha_{\rm s}) = \frac{Q^2}{\hat{s}} \sum_q \delta_{aq}\delta_{b\bar{q}}\sigma^{(0)}_{q\bar{q}\to Z} \int_0^\infty db \frac{b}{2} J_0(bq_{\rm T}) \exp\big\{ L g_q^{(1)}(\alpha_s L)\big\}, \tag{67}$$

where

$$g_q^{(1)}(\alpha_s L) = \frac{A_q^{(1)}}{\beta_0}\frac{\lambda + \ln(1-\lambda)}{\lambda} \tag{68}$$

with $\lambda = \frac{1}{\pi}\beta_0\alpha_s L$, $\beta_0 = (11C_A - 2N_f)/12$ being the zeroth order beta function and $A_q^{(1)} = C_F$. As is defined in chapter 3, $\alpha_{\rm s} \equiv \alpha_{\rm s}(\mu_{\rm R}^2)$ and $L \equiv \ln\frac{M^2 b^2}{b_0^2}$.

For the NLL accuracy, there will be finite part corrections. The finite part is given by the leading order QCD correction (which is the order of $\alpha_{\rm s}^1$), say totally as NLL+LO accuracy

$$\left[\frac{d\hat{\sigma}_{ab}^{\rm Z,(fin.)}}{dq_{\rm T}^2}\right]_{\rm LO} = \left[\frac{d\hat{\sigma}_{ab}^{\rm Z}}{dq_{\rm T}^2}\right]_{\rm LO} - \left[\frac{d\hat{\sigma}_{ab}^{\rm Z,(res.)}}{dq_{\rm T}^2}\right]_{\rm LO}. \tag{69}$$

$\left[d\hat{\sigma}_{ab}^{\rm Z}/dq_{\rm T}^2\right]_{\rm LO}$ is given by only the real emission correction in Eq. (28), since the $\delta(q_{\rm T}^2)$ contribution from virtual correction has been removed. Explicit forms of $\left[d\hat{\sigma}_{ab}^{\rm Z,(res.)}/dq_{\rm T}^2\right]_{\rm LO}$ can be found in [35].

The resummation part of NLL accuracy is

$$\frac{d\hat{\sigma}_{ab}^{\rm Z,(res.),NLL}}{dq_{\rm T}^2}(q_{\rm T}, Q, \hat{s}; \alpha_{\rm s}, \mu_{\rm R}^2, \mu_{\rm F}^2) = \frac{Q^2}{\hat{s}}\int_0^\infty db\frac{b}{2}J_0(bq_{\rm T})\mathcal{W}_{ab}^{\rm Z,NLL}(b, Q, \hat{s}; \alpha_s, \mu_{\rm R}^2, \mu_{\rm F}^2), \tag{70}$$

where the N-moments function of $\mathcal{W}_{ab}^{\rm Z,NLL}$ is explicitly calculated as

$$\begin{aligned}\mathcal{W}_{ab,N}^{\rm Z,NLL}(b, M; \alpha_s, \mu_{\rm R}^2, \mu_{\rm F}^2) = \sum_{\rm q}\mathcal{H}_{ab,N,q}^{\rm Z,NLL}(Q, \alpha_s; Q^2/\mu_{\rm R}^2, Q^2/\mu_{\rm F}^2, Q^2/M^2) \\ \exp\left\{Lg_q^{(1)}(\alpha_s L) + g_{q,N}^{(2)}(\alpha_s L; M^2/\mu_{\rm R}^2, M^2/Q^2)\right\},\end{aligned} \tag{71}$$

where

$$\begin{aligned}&\mathcal{H}_{ab,N,q}^{\rm Z,NLL}(Q, \alpha_s; Q^2/\mu_{\rm R}^2, Q^2/\mu_{\rm F}^2, Q^2/M^2) \\ &\quad = \sigma_{q\bar{q}\to Z}^{(0)}(M)\Bigg\{1 + \frac{\alpha_s}{\pi}\big[\delta_{aq}\delta_{b\bar{q}}\mathcal{H}_{q\bar{q}\leftarrow q\bar{q},N}^{(1)}(Q^2/\mu_{\rm F}^2, Q^2/M^2) \\ &\qquad\qquad + \delta_{aq}\delta_{bg}\mathcal{H}_{q\bar{q}\leftarrow qg,N}^{(1)}(Q^2/\mu_{\rm F}^2, Q^2/M^2) \\ &\qquad\qquad + \delta_{ag}\delta_{bq}\mathcal{H}_{q\bar{q}\leftarrow gq,N}^{(1)}(Q^2/\mu_{\rm F}^2, Q^2/M^2)\big]\Bigg\},\end{aligned} \tag{72}$$

$$g_{q,N}^{(2)}(\alpha_s L; Q^2/\mu_{\rm R}^2, Q^2/M^2) = -\frac{A_q^{(2)}}{\beta_0^2}\Big(\frac{\lambda}{1-\lambda}+\ln(1-\lambda)\Big) + \frac{A_q^{(1)}}{\beta_0}\Big(\frac{\lambda}{1-\lambda}+\ln(1-\lambda)\Big)\ln\frac{M^2}{\mu_{\rm R}^2} + \frac{A_q^{(1)}\beta_1}{\beta_0^3}\Big(\frac{\lambda}{1-\lambda}+\frac{\ln(1-\lambda)}{1-\lambda}+\frac{1}{2}\ln^2(1-\lambda)\Big) + \frac{\bar{B}_{q,N}^{(1)}}{\beta_0}\ln(1-\lambda), \tag{73}$$

and the related perturbative coefficients are

$$\begin{aligned} A_q^{(2)} &= \frac{1}{2}C_F\bigg[\Big(\frac{67}{18}-\frac{\pi^2}{6}\Big)C_A - \frac{5}{9}N_f\bigg], \\ B_q^{(1)} &= -\frac{3}{2}C_F, \\ \bar{B}_{q,N}^{(1)} &= \tilde{B}_{q,N}^{(1)} + A_q^{(1)}\ln\frac{Q^2}{M^2} = B_q^{(1)} + 2\gamma_{qq,N}^{(1)} + A_q^{(1)}\ln\frac{Q^2}{M^2}, \end{aligned} \tag{74}$$

and the first order β-function is

$$\beta_1 = \frac{1}{24}(17C_A^2 - 5C_A N_f - 3C_F N_f). \tag{75}$$

According to [37], the perturbative coefficients in Eq. (72) are

$$\begin{aligned} \mathcal{H}_{q\bar{q}\leftarrow q\bar{q},N}^{(1)}(Q^2/\mu_{\rm F}^2, Q^2/M^2) &= C_F\big(\frac{1}{N(N+1)} - 4 + \frac{\pi^2}{2}\big) - \big(B_q^{(1)} + \frac{1}{2}A_q^{(1)}\ln\frac{Q^2}{M^2}\big)\ln\frac{Q^2}{M^2} \\ &\quad + 2\gamma_{qq,N}^{(1)}\ln\frac{Q^2}{\mu_{\rm F}^2}, \\ \mathcal{H}_{q\bar{q}\leftarrow gq(qg),N}^{(1)}(Q^2/\mu_{\rm F}^2, Q^2/M^2) &= \frac{1}{2(N+1)(N+2)} + \gamma_{gq(qg),N}^{(1)}\ln\frac{M^2}{\mu_{\rm F}^2}, \end{aligned} \tag{76}$$

where the LO parton anomalous dimensions are [14]

$$\begin{aligned} \gamma_{qq,N}^{(1)} &= C_F\bigg[-\frac{1}{2} + \frac{1}{N(N+1)} - 2\sum_{k=2}^{N}\frac{1}{k}\bigg], \\ \gamma_{qg,N}^{(1)} &= \frac{1}{2}\frac{2+N+N^2}{N(N+1)(N+2)}, \\ \gamma_{gq,N}^{(1)} &= C_F\frac{2+N+N^2}{N(N^2-1)}. \end{aligned} \tag{77}$$

As is stated in chapter 3, to give kinematic corrections to the large $q_{\rm T}$ region, the variable L should be replaced by $\tilde{L}$ for all form factors above.

There is a singularity for the form factor near the Landau poles of QCD. To regularize such singularities, the inverse Fourier transform from b-space back to $p_{\rm T}$-space should be extend to the complex b-plane and choose special integration contours. Such a strategy is called minimal prescription'. We followed the explicit method proposed in [39] in our calculation. Firstly, the Bessel function is splitted into two auxiliary functions

$$\begin{aligned} h_1(z,v) &\equiv -\frac{1}{\pi}\int_{-iv\pi}^{-\pi+iv\pi} d\theta e^{-iz\sin\theta} \\ h_2(z,v) &\equiv -\frac{1}{\pi}\int_{\pi+iv\pi}^{-iv\pi} d\theta e^{-iz\sin\theta}. \end{aligned} \tag{78}$$

Then the Fourier transform in Eq. (53) becomes

$$\begin{aligned} \frac{d\sigma^{(\rm res.)}_{{\rm F},ab}}{dp_{\rm T}^2}(p_{\rm T},Q,\hat{s};\alpha_s(\mu_{\rm R}^2),\mu_{\rm R}^2,\mu_{\rm F}^2) = \frac{M^2}{\hat{s}}\big[\int_{C_1} db\frac{b}{4}h_1(bq_{\rm T}) + \int_{C_2} db\frac{b}{4}h_2(bq_{\rm T})\big] \\ \mathcal{W}^{\rm F}_{ab}(b,Q,\hat{s};\alpha_s(\mu_{\rm R}^2),\mu_{\rm R}^2,\mu_{\rm F}^2), \end{aligned} \tag{79}$$

where

$$\begin{aligned} C_1:\ b = b_c - tE^{-i\phi_b}(0<b<\infty) \\ C_2:\ b = b_c - tE^{i\phi_b}(0<b<\infty). \end{aligned} \tag{80}$$

The value of b_c and ϕ_b are chosen to avoid the Laudau pole.

The inverse Mellin transform from the N-space to z-space is of the formula

$$\mathcal{W}^{\rm F}_{ab}(b,Q,Q^2/z;\alpha_s(\mu_{\rm R}^2),\mu_{\rm R}^2,\mu_{\rm F}^2) = \int_C \frac{dN}{2\pi i} z^{-N}\mathcal{W}^{\rm F}_{ab,N}(b,Q;\alpha_s(\mu_{\rm R}^2),\mu_{\rm R}^2,\mu_{\rm F}^2), \tag{81}$$

where C is the integration contour on the complex N-plane. To give better numerical convergence, we choose the contour to be [58]

$$N = C + te^{i\phi}, \tag{82}$$

with $0 \le t \le \infty$. For arbitrary $C > 0$ and $\pi > \phi > \pi/2$, the integration is convergent for the dual parameter $z = Q^s/\hat{s} < 1$. Moreover, there is

a singularity at $\rho_L = \exp[1/(2b_0\alpha_s)]$ in the resummed cross section, which introduces a power-suppressed ambiguity in the transformation. To solve the problem, it is in addition chosen to be $C < \rho_L$.

To further improve the numerical convergence, we used the method in [59] to transform PDF functions into the N-space first. The function used to fit the PDF's is $x^\alpha(1-x)^\beta$, which corresponds to the beta functions $B(\alpha+N, \beta-1)$ in the N-space.

Finally in summary, the resummed part of the total differential cross section is

$$\frac{d\sigma^{\mathrm{Z,(res.)}}_{\mathrm{h_A h_B}}}{dq_{\mathrm{T}}^2}(q_{\mathrm{T}}, s) = \int_0^1 dz\delta(z - \frac{Q^2}{s}) \int_C \frac{dN}{2\pi i} z^{-(N-1)} \frac{d\sigma^{\mathrm{Z,(res.)}}_{\mathrm{h_A h_B,N}}}{dq_{\mathrm{T}}^2}(q_{\mathrm{T}}), \tag{83}$$

where

$$\begin{aligned}\frac{d\sigma^{\mathrm{Z,(res.)}}_{\mathrm{h_A h_B,(N+1)}}}{dq_{\mathrm{T}}^2}(q_{\mathrm{T}}) = \sum_{a,b}\Big[\int_{C_1} db \frac{b}{4} h_1(bq_{\mathrm{T}}) + \int_{C_2} db \frac{b}{4} h_2(bq_{\mathrm{T}})\Big] \\ f_{\mathrm{a/h_A,N}}(\mu_{\mathrm{F}}^2) f_{b/h_B,N}(\mu_{\mathrm{F}}^2) \mathcal{W}^{\mathrm{F}}_{ab,N}(b, Q; \alpha_s, \mu_{\mathrm{R}}^2, \mu_{\mathrm{F}}^2).\end{aligned} \tag{84}$$

The same approach can be used to calculate the resummation contribution of fixed order to extract finite part differential cross section.

In calculations, the factorization scale μ_{F} will affect the resummed result. Fig. 10 is the resummed differential cross sections with different factorization scales at NLL accuracy.

Different choices of PDF set can also affect the distributions. Fig. 11 is the comparison between our NLL result, which used the CTEQ 6 PDF, and the ResBos [60] result, which used the CT10 PDF. The small discrepancy between two curves at very low q_{T} region is due to non-perturbative effects.

5.3 Logarithmic Resummed Accuracy of Pythia8 Prediction for Transverse Momentum Distribution

We used Pythia8 event generator to give the parton shower prediction of Z boson transverse momentum distribution for Drell Yan process.

The FSR and ISR of Pythia8 are based on the q_{T}-ordered dipole approach. The approach has been introduced in section 5.1. It is supposed to reach the NLL accuracy for logarithmic resummation. However, the splitting kernels used in Pythia8 are first order DGLAP kernels. Using such kernels, the

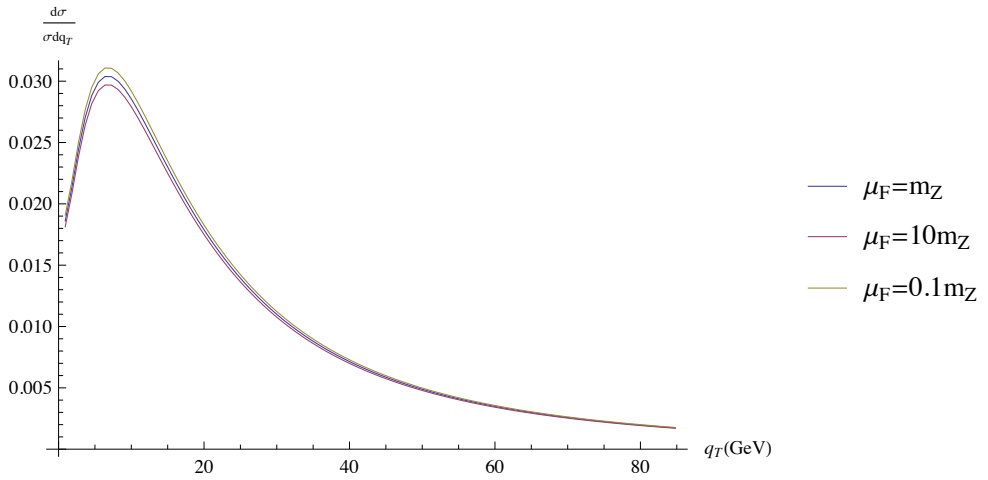

Figure 10: Resummation of Z boson transverse momentum distribution for Drell Yan process at NLL accuracy with different factorization scales at $E_{\rm CM} = 14$TeV.

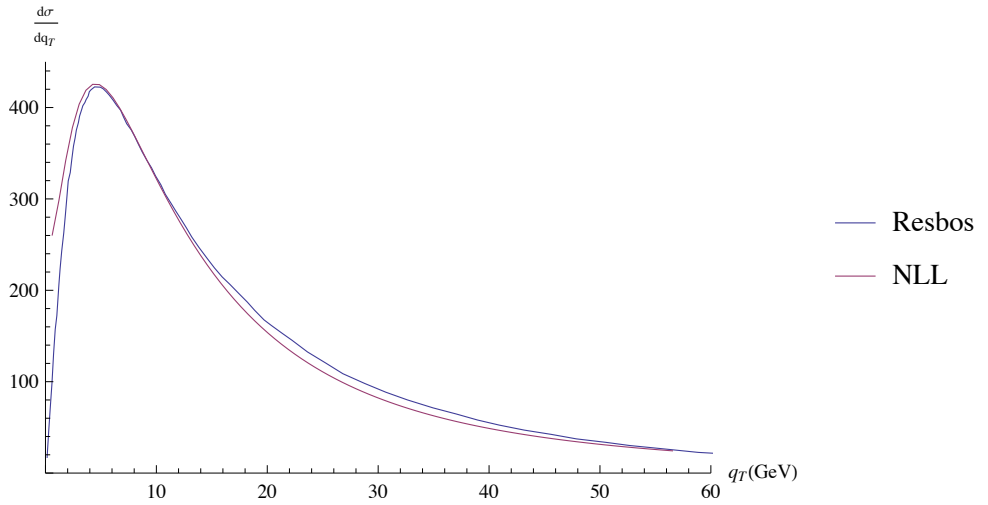

Figure 11: Comparison with the ResBos NLL resummation of the Z boson transverse momentum distribution for Drell Yan process: $E_{\rm CM} = 14$TeV, $\mu_{\rm F} = m_{\rm Z}$

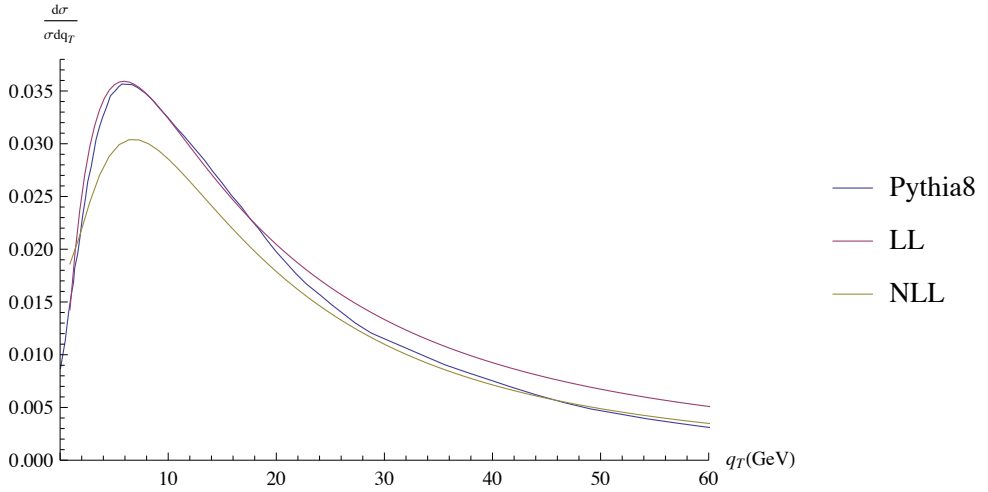

Figure 12: Numerical comparison between the Pythia8 prediction and the resummation predictions at LL and NLL accuracy with $E_{\mathrm{CM}} = 14\mathrm{TeV}$.

analytical expressions of q_{T} distribution for FSR and ISR are still the leading logarithm resummation formalism [61].

Pythia8 has also implemented a leading order ME correction to its PS algorithm. An internal ME correction to the ISR has been performed to $2 \to 1$ processes like the Z boson production.

Fig. 12 is the numerical comparison between the Pythia8 prediction and the resummation prediction at LL and NLL accuracy. It can be seen that the Pythia8 prediction matches LL accuracy in low q_{T} region better, while in the large q_{T} region, it fits the NLL result very well.

Chapter 6 Conclusion

In this thesis, we focused on the transverse momentum distribution of Z boson for Drell Yan process. The distribution can be predicted by perturbative QCD. In the first chapter, we introduced the theoretical backgrounds of quantum chromodynamics and its perturbative method. Then in the next chapter, we gave a description of the Drell Yan process, its kinematics and the factorization theory for the process.

We also calculated explicitly the first order QCD corrections to the transverse momentum distribution for the process. The calculation shows that logarithmic divergences emerge in such an semi-inclusive quantity at very small q_{T}. Such divergences are originated from the soft and collinear structure of QCD hard processes. For inclusive quantities, the soft and collinear singularities can be factorized into the parton distribution functions, which is the factorization theorem introduced before. However, as the q_{T} distribution is semi-inclusive, further methods need to be introduced to deal with the logarithmic divergences in order to keep the perturbative argument valid.

Transverse momentum resummation can solve the problem by summing over logarithmic terms systematically. In chapter 3, we introduced different approaches and formalisms of resummation. The resummation can be done either in q_{T}-space or its Fourier conjugate b-space. It is easier to do higher level logarithmic resummation in b-space however certain matching procedure between high q_{T} and low q_{T} region are needed in this case.

Another approach usually used in Monte Carlo event generators is a parton shower algorithm. PS simulate the soft and collinear radiations for the hard process of QCD. We introduced the algorithm in chapter 4 and further explored its logarithmic resummation accuracy in chapter 5.

According to the numerical result, the prediction made by Pythia8 event generator matches the LL accuracy at low q_{T} better. However, Pythia8 implemented ME corrections, which may have given the prediction better high q_{T} behavior. The numerical comparison shows that the high q_{T} behavior of Pythia8 prediction fits the NLL+LO resummation results very well.

References

[1] M.Y. Han and Y. Nambu, Phys. Rev. 139, B1006 (1965);

[2] Greenberg, O.W., Phys. Rev. Lett. 13, 598 (1964);

[3] Gross, D.J., and F. Wilczek, Phys. Rev. Lett. 30, 1343 (1973);

[4] Politzer, H.D., Phys. Rev. Lett. 30, 1346 (1973);

[5] Feynman, R.P., Phys. Rev. Lett. 23, 1415 (1969);

[6] Bjorken, J.D., Phys. Rev. 179, 1547 (1969);

[7] Bloom, E.D., D.H. Coward, H. DeStaebler, J. Drees, G. Miller, L.W. Mo, R.E. Taylor, M. Brei- denbach, J.I. Friedman, G.C. Hartmann, and H.W. Kendall, Phys. Rev. Lett. 23, 930 (1969);

[8] Breidenbach, M., J.L. Friedman, H.W. Kendall, E.D. Bloom, D.H. Coward, H. DeStaebler, J. Dress, L.W. Mo, and R.E. Taylor, Phys. Rev. Lett. 23, 935 (1969);

[9] Friedman, J.I., and H.W. Kendall, Ann. Rev. Nucl. Part. Sci. 22, 203 (1972);

[10] Collins, J.C., D.E. Soper, and G. Sterman, *Perturbative Quantum Chromodynamics*, (1989);

[11] S.D. Drell and T.-M. Yan, Phys. Rev. Lett. 25, 316 (1970);

[12] R. Hamberg, W.L. van Neerven, T. Matsuura, Nucl. Phys. B 359, 343 (1991); R. Hamberg, W.L. van Neerven, T. Matsuura, Nucl. Phys. B 644, 403, Erratum (2002); R.V. Harlander, W.B. Kilgore, Phys. Rev. Lett. 88, 201801(2002);

[13] C. Anastasiou, L.J. Dixon, K. Melnikov, F. Petriello, Phys. Rev. D 69, 094008 (2004);

[14] R.K. Ellis, W.J. Stirling and B.R. Webber, *QCD and Collinder Physics*, Cambridge University Press;

[15] J.C. Collins and D.E. Soper, Ann. Rev. Nucl. Part. Sci. 37, 383 (1987);

[16] Gribov, V.N., and L.N. Lipatov, Yad. Fiz. 15, 781 (Sov. J. Nucl. Phys. 15, 438) (1972);

[17] Altarelli, G., and G. Parisi, Nucl. Phys. B126, 298 (1977);

[18] R.K. Ellis, G. Martinelli, R. Petronzio, Nucl. Phys. B 211, 106 (1983);

[19] P.B. Arnold, M.H. Reno, Nucl. Phys. B 319, 37 (1989); P.B. Arnold, M.H. Reno, Nucl. Phys. B 330, 284, Erratum (1990);

[20] R.J. Gonsalves, J. Pawlowski, C.F. Wai, Phys. Rev. D 40, 2245 (1989);

[21] Particle Data Group;

[22] M.E. Peskin and D.V. Schroeder, *An Introduction to Quantum Field Theory*, (1995);

[23] J. C. Collins, *Foundations of Perturbative QCD* (Cambridge University Press, Cambridge, 2011);

[24] J. Collins, J.-W. Qiu, Phys. Rev. D75, 114014 (2007); J. C. Collins, A. Metz, Phys. Rev. Lett. 93, 252001 (2004);

[25] Yu.L. Dokshitzer, D.I. Dyakonov and S.I. Troyan, Phys. Lett. 78B 290 (1978); Phys. Rep. 58, 269 (1980);

[26] S.D. Ellis, N. Fleishon, and W.J. Stirling, Phys. Rev. D 24, 5 (1981);

[27] G. Parisi, R. Petronzio, Nucl. Phys. B 154, 3 (1979);

[28] G. Curci, M. Greco, Y. Srivastava, Nucl. Phys. B 159, 3 (1979);

[29] J.C. Collins, D. E. Soper, G. Sterman, Nucl. Phys. B 250, 1 (1985);

[30] J.C. Collins, D. Soper, Nucl. Phys. B 193, 381 (1981); B 213, 545 (E) (1983); B 197, 446 (1982);

[31] R.K. Ellis, Sinia Veseli, Nucl. Phys. B 511, 649 (1998);

[32] Nuclear Physics B 596, 299-312: 307 (2001);

[33] D. de Florian, M. Grazzini, hep-ph/0008152;

[34] S. Catani, D. de Florian, M. Grazzini, Nucl. Phys. B 596, 299 (2001);

[35] G. Bozzi, S. Catani, D. de Florian and M. Grazzini, Nucl. Phys. B 737, 73 (2006);

[36] G. Bozzi, S. Catani, G. Ferrera, D. de Florian and M. Grazzini, Phys. Lett. B 696, 207 (2011);

[37] G. Bozzi, S. Catani, G. Ferrera, D. de Florian, M. Grazzini, Nucl. Phys. B, 815, 174-197 (2009);

[38] S. Catani, M.L. Mangano, P. Nason, L. Trentadue, Nucl. Phys. B 478, 273 (1996)

[39] A. Kulesza, G. Sterman, W. Vogelsang, Phys. Rev. D 69, 014012 (2004)

[40] M. Dasgupta, G.P. Salam, Eur. Phys. J. C 24, 213 (2002); M. Dasgupta, G.P. Salam, JHEP 0208, 032 (2002);

[41] G. Marchesini and B.R. Webber, Nucl. Phys. B310, 461 (1988); S. Gieseke, P. Stephens, and B. Webber, JHEP 0312, 045 (2003)

[42] M. Bengtsson and T. Sjostrand, Nucl. Phys. B 289, 810 (1987);

[43] G. Gustafson, U. Pettersson, Nucl. Phys. B 306, 746 (1988);

[44] S. Catani *et al.*, JHEP 11, 063 (2001), hep-ph/0109231;

[45] S. Frixione and B.R. Webber, JHEP 06, 029 (2002), hep-ph/0204244;

[46] P. Nason, JHEP 11, 040 (2004), hep-ph/0409146;

[47] S. Alioli *et al.*, JHEP 1006, 043 (2010), arXiv:1002.2581;

[48] T. Sjostrand, P.Z. Skands, Eur. Phys. J. C 39, 129154 (2005);

[49] S. Catani, M.H. Seymour, Nucl. Phys. B 485, 291419 (1997);

[50] A. Buckley, *et al.*, Phys. Rep. 504, 145-233 (2011);

[51] M.Bahr *et al.*, Eur. Phys. J. C 58, 639 (2008), arXiv:0803.0883;

[52] T. Sjostrand, S. Mrenna, and P. Z. Skands, Comp. Phys. Comm. 178, 852 (2008), arXiv:0710.3820;

[53] T. Gleisberg *et al.*, JHEP 0402, 056 (2004), hep-ph/0311263;

[54] J. Beringer *et al.* (PDG), Phys. Rev. D 86, 010001 (2012) (http://pdg.lbl.gov);

[55] T. Sjostrand, Phys. Lett. B 157, 321 (1985);

[56] E. Norrbin and T. Sjostrand, Nucl. Phys. B 603, 297 (2001), hep-ph/0010012;

[57] S. Catani *et al.*, Nucl. Phys. B 627, 189 (2002), hep-ph/0201036;

[58] A. Kulesza, G. Sterman, and W. Vogelsang, Phys. Rev. D 66, 014011 (2002);

[59] D. de Florian and J. Zurita, Phys. Lett. B 659, 813 (2008);

[60] G.A. Ladinsky and C.-P. Yuan, Phys. Rev. D 50, 4239 (1994); C. Balazs, Jian-wei Qiu, C.-P. Yuan. Phys. Lett. B 355, 548-554 (1995); C. Balazs, C.-P. Yuan, Phys. Rev. Lett. 79, 2398-2401 (1997); C. Balazs, C.-P. Yuan, Phys. Rev. D 56, 5558-5583 (1997); F. Landry, R. Brock, P.M. Nadolsky, C.-P. Yuan. Phys. Rev. D 67, 073016 (2003);

[61] T. Sjostrand, *et al.*, Computer Physics Communications, 191, Pages 159-177 (2015);